ORNL/TM-2000/212

R-MATRIX EVALUATION OF ^{16}O NEUTRON CROSS SECTIONS UP TO 6.3 MEV

R. O. SAYER, L. C. LEAL, N. M. LARSON,
R. R. SPENCER, AND R. Q. WRIGHT

August 2000

ORNL/TM-2000/212

Computational Physics and Engineering Division

R-Matrix Evaluation of ^{16}O Neutron Cross Sections up to 6.3 MeV

R. O. Sayer
L. C. Leal
N. M. Larson
R. R. Spencer
R. Q. Wright

Date Published: August 2000

Prepared by the
OAK RIDGE NATIONAL LABORATORY
Oak Ridge, Tennessee 37831
managed by
UT-BATTELLE, LLC
for the
U.S. DEPARTMENT OF ENERGY
under contract DE-AC05-00OR22725

CONTENTS

LIST OF FIGURES

LIST OF TABLES

R-Matrix Evaluation of ^{16}O Neutron Cross Sections up to 6.3 MeV

R. O. Sayer, L. C. Leal, N. M. Larson, R. R. Spencer, and R. Q. Wright

1. Introduction

In this paper we describe an evaluation of ^{16}O neutron cross sections in the resolved resonance region with the multilevel Reich-Moore R-matrix formalism. Resonance analyses were performed with the computer code SAMMY [LA98] which utilizes Bayes' method, a generalized least squares technique.

Over the years the nuclear community has developed a collection of evaluated nuclear data for applications in thermal, fast reactor, and fusion systems. However, typical neutron spectra in criticality safety applications are different from the spectra relevant to thermal, fast reactor, and fusion systems. In fact, the neutron spectra important for these non-reactor systems appear to peak in the epithermal energy range. Nuclear data play a major role in the calculation of the criticality safety margins for these systems. A thorough examination of how the present collection of nuclear data evaluations behaves in criticality safety calculations is needed. Many older evaluations will probably need to be revised, and new evaluations will be needed.

Oxygen is an important element in criticality safety applications where oxides are present in significant abundance. The existing ENDF/B-VI.5[**] evaluation is expressed in terms of point-wise cross sections derived from the analysis of G. Hale [HA91]. Unfortunately such an evaluation is not directly useful for resonance analysis of data from samples in which oxygen is combined with other elements; for that purpose, Reich-Moore resonance parameters are needed. This paper addresses the task of providing those parameters. In the following sections we discuss the data, resonance analysis procedure, and results.

[**] ENDF/B-VI Release 5 (September, 1998)

2. Total and Reaction Cross Section Data

An extensive search of standard nuclear databases and the open literature led to selection of total, reaction, and angle differential elastic cross section data sets for the analysis. Selected information about these data sets is listed in Table 1 for total and reaction data and in Table 2 for differential elastic data.

The total cross section data include measurements by Johnson, et al. [JO74], on the 200-m flight path at the Oak Ridge Linear Accelerator (ORELA); Cierjacks, et al. [CI80], on the 200-m flight path at the Karlsruhe Isochronous Cyclotron; Larson [LA80] (ORELA 80 m flight path); Fowler, et al. [FJF73], who utilized a flight path of 47 m and a pulsed van de Graaff accelerator to produce neutrons; and Johnson, et al. [JO80], who made very accurate measurements in the 2.35 MeV window region. In the energy range of overlap, 600 - 4300 keV, the total cross section values for Refs [JO74, LA80, FJF73] are in good agreement, but the data of Cierjacks, et al. [CI80] is about 3% lower. The Cierjacks data were normalized to the data of Johnson, et al. [JO74], by integrating over the energy range 3450 to 3720 keV. The normalization factor was 1.035. To make the JO74 peak energies consistent with the higher resolution CI80 values, we applied the following neutron energy transformation to the data of Johnson, et al. [JO74] :

$$E = E_O - 0.00462\, E_O^{0.5} + 0.0000146\, E_O^{1.5}$$

This relation gives shifts of 0.3 keV at 1 MeV, 2.2 keV at 3 MeV, and 4.8 keV at 5 MeV.

The ^{16}O (n, α)^{13}C channel opens at E_n = 2360 keV and contributes about 9% to σ_{total} at E_n = 4180 keV and about 25% at 5070 keV. Therefore, $\sigma_{n,\alpha}$ values deduced by reciprocity from $^{13}C(\alpha, n)^{16}O$ measurements by Bair and Haas [BH73] were fit to obtain Γ_α values for several resonances. These data exhibit good α energy resolution of 2 to 5 keV over the energy range corresponding to the neutron energies of interest for this evaluation. Energy transformations were applied to the data of Bair and Haas to align the narrow resonances with the more precise energies of Cierjacks, et al.

Although the absolute uncertainties are rather large (±20%), the BH73 $^{13}C(\alpha, n)$ cross section data are 40-50% larger than the $^{13}C(\alpha, n)$ data of Sekharan, et al. [SE67] and about 30% larger than the $^{16}O(n, \alpha)$ data of Walton, et al. [WCB57]. The reasons for these large differences are not understood. However, the BH73 data agree to better than 10% with the recent high-precision measurements of Drotleff, et al. [DR93] in the region of overlap, E_n = 3200 to 3480 keV. Therefore, we analyzed both the BH73 and DR93 data sets, applying a single normalization factor, $F_{n\alpha}$, that was varied in the SAMMY fits. The analysis procedure is discussed further in section 4.

In order to give a proper treatment for charged particles in an exit channel, an algorithm [SA00] to calculate charged particle penetrabilities (CPP) and shifts was incorporated in the SAMMY code. A slightly modified version of the routine COULFG of Barnett [BA91] is used to compute the Coulomb wave functions and their derivatives. The methodology for CPP computation is presented in the Appendix. Routines based on the CPP algorithm will be developed and proposed for incorporation in future versions of the nuclear data processing codes AMPX [GR92] and NJOY [MA94].

Fig. 1 presents a global view of the final SAMMY fits to the reaction data of BH73 and the total cross section data of FJF73, JO74, CI80, JO80, LA80, and OH84.

3. Angle Differential Elastic Data

Angle differential elastic cross sections were computed with SAMMY using the set of resonance parameters obtained from analysis of the total and reaction cross section data. These predicted values were compared with angular distribution data [Refs OK55, FC58, PH60, MZ62, HH62, JF67, FJ70, KP72, and DR76] in order to confirm angular momentum values for several resonances. Predicted Legendre coefficients were compared with the corresponding experimental values of Lister and Sayres [LS66] . Fig. 2 depicts the energies for which angle differential data were available on a plot of total cross section vs. neutron energy.

4. Resonance Analysis

Resonance parameters were determined by a consistent analysis in which both Doppler and resolution broadening effects were incorporated. Results from a preliminary ^{16}O evaluation have been reported previously [LE98].

Total and reaction data sets listed in Table 1 were analyzed sequentially with the SAMMY code so that each fit was connected to the previous fit by the parameter covariance matrix [LA98] . In this manner energies and widths were determined for 37 resonances in the range $0.2 < E_n < 6.3$ MeV. Two negative-energy resonances were included to account for bound levels and 13 high-energy resonances were included to account for the effect of resonances above 6.3 MeV. Partial waves $\mathbf{s_{1/2}}$ through $\mathbf{g_{9/2}}$ were included in the analysis. The neutron channel radius, $\mathbf{a_n}$, α channel radius, $\mathbf{a}_\alpha$, and the $\sigma_{n,\alpha}$ normalization factor, $F_{n\alpha}$, were varied to improve the agreement between theory and experiment. Final values were $\mathbf{a_n} = 3.80$ fm, $\mathbf{a}_\alpha = 6.7$ fm, and $F_{n\alpha} = 1.00$.

Spin-parity assignments were based on fits to total and reaction cross section data and on comparison of predicted and experimental $d\sigma/d\Omega$ values. In cases where fits were

inconsistent with the data, several $\mathbf{J}^{\pi}$ values were tried to improve the fits. For most resonances our $\mathbf{J}^{\pi}$ values are identical to those reported in the compilation by Tilley, et al. [TI93]. Exceptions are discussed in the following section.

As indicated in Table 2, the experimental energy resolution values for the differential elastic data vary over a wide range. Predicted $d\sigma/d\Omega$ values were energy-broadened by the appropriate amount before comparison with the data. An example of the effect of energy broadening is given in Fig. 3 for the data of FJ70 for the 1834 keV $\mathbf{d_{3/2}}$ resonance (ΔE = 13 keV, Γ = 7.8 keV), and for the 3211- and 3443-keV resonances. Solid and dashed curves represent the broadened and unbroadened predictions, respectively.

5. Results

Examples of SAMMY fits to the total cross section data of JO74, JO80, and CI80 are presented in Figs. 4, 5, and 6, respectively.

The $\sigma_{n,\alpha}$ cross sections obtained by reciprocity from the Bair and Haas [BH73] **(α, n)** data and the SAMMY fit are shown in Fig. 7. Similarly, the data of Drotleff, et al. [DR93], also deduced from reciprocity, and the SAMMY fit are shown in Fig. 8.

A rather large α channel radius, 6.7 fm, was required in order to fit the (n, α) data because the 3291 keV $d_{3/2}$ resonance (Γ_n = 340 keV, Γ_α = 0.17 keV) introduces a significant "background" for $E_n > 4.5$ MeV. This is due to the exponential increase of the Coulomb penetrability, and hence Γ_α, with E_n. As can be been from Figs. 7 and 8, the agreement between predicted and experimental (n, α) values is quite satisfactory over the fit range 3100 to 6300 keV. At lower energies, where the cross section is orders of magnitude smaller, the prediction underestimates $\sigma_{n,\alpha}$.

Angle differential elastic data from Refs. [OK55, FC58, PH60, MZ62, JF67, FJ70, KP72, and DR76] are compared with SAMMY predictions in Figs. 9, 10, 11, 12, and 13. In general there is good agreement between experiment and predictions. Legendre coefficients given by LS66 are compared with predicted values in Fig. 14. When uncertainties are taken into account, predicted and experimental coefficients are in satisfactory agreement.

Below 3500 keV the contribution to σ_{total} from the α channel is less than 0.01 b. However, $\sigma_{n,\alpha}$ is about 9% of σ_{total} at E_n = 4180 keV and about 25% at E_n = 5070 keV. It is assumed that the extraction of $d\sigma/d\Omega$ (nn) and Legendre coefficients from the experimental measurements was not affected by competition from the α channel.

Caro [CA98] has reported an evaluation of ^{16}O using a resonance plus potential well model which, unfortunately, does not provide a resonance parameter representation. In Fig. 15, we compare our predicted $d\sigma/d\Omega$ values with Caro and ENDF/B-VI.5 for four non-resonant energies: 1.50, 1.75, 2.56, and 2.76 MeV. At these energies the differences in predicted values are small except at forward angles, where the two recent evaluations give better agreement with experiment than does ENDF/B-VI.5.

In Table 4 we list the level number, the ^{17}O level excitation energy $E_{\mathbf{x}}$, peak energy $E_{\mathbf{peak}}$, resonance energy $E_{\mathbf{r}}$, neutron width $\Gamma_{\mathbf{n}}$, alpha width Γ_α, and J^π value for resonances included in the present evaluation. An asterisk denotes a J^π value that is different from the assignment of TI93. A negative sign for Γ_α indicates that the product of reduced widths $\gamma_{\mathbf{n}}\gamma_\alpha$ is negative. For a particular partial wave, e.g., $\mathbf{d_{3/2}}$, peak energies are defined as those energies corresponding to maxima in the unbroadened partial cross section for that partial wave. For the $\mathbf{s_{1/2}}$ partial wave, the $E_{\mathbf{peak}}$ values correspond to minima in the unbroadened s-wave partial cross section. Excitation energies are computed from the separation energy and nuclear masses A_n and A_{O16} according to:

$$E_X = 4143.36 \text{ keV} + E_r * A_{O16}/(A_{O16} + A_n)$$

The resonance energies $E_{\mathbf{r}}$ in Table 4 correspond to the eigenenergies determined by the Reich-Moore analysis with SAMMY with boundary conditions chosen so that the level shifts are zero.

5.1. $0 < E_n < 3100$ keV

Resonance energies E_r and neutron widths Γ_n were determined for 10 levels in the energy range $0 < E_n < 3100$ keV, where the contribution to σ_{total} from $\sigma_{\mathbf{n},\alpha}$ is completely negligible (see Fig. 8). Below the first unbound level at 434 keV we obtained excellent fits to both the ORELA 200-m data [JO74] and the data of Ohkubo [OH84] as shown in Fig. 1. In the following discussion a resonance is denoted by the level number, J^π value, and resonance energy E_r. Levels 1 and 2 are fictitious resonances to account for the effect of bound levels.

Levels 3, 4, and 5 are based primarily on fits to the ORELA 200-m data [JO74]. Parameters for Levels 6, 8, and 9 were obtained by fitting the ORELA data and the data of FJF73, who used a Van de Graaff accelerator to produce neutrons via the (p, n) reaction. Our energies, widths, and J^π values for these six levels are consistent with TI93. For levels 3, 4, and 8, our predicted $d\sigma/d\Omega$ values are in good agreement with the data of OK55, FC58, and FJ70, respectively.

Level 7. ($5/2^-$), 1689 keV. Assuming $J^\pi = 5/2^-$, we obtain a neutron width of 0.27 keV from fits to the JO74 σ_{total} data, which has an energy resolution of 1.7 keV at 1689 keV. This level is also observed by FJF73 but with poorer energy resolution. J^π is not $1/2^+$ since that would produce a dip, not a peak, in σ_{total} . TI93 gives $J^\pi = (5/2^-)$. On the basis of their (e, e') measurements, Manley, et al. [MA87] conclude that this level has negative parity and spin between 1/2 and 11/2. They suggest $J^\pi = 5/2^-$ because the B(E3) value of 134 e^2fm^6 is large. For J = 1/2, 3/2, 5/2, 7/2, and 9/2, our fits give Γ_n= 0.56, 0.36, 0.27, 0.22, and 0.18 keV, respectively.

Level 10. $1/2^+$, 2377.9 keV. The width and energy are primarily determined by the high-precision JO80 data corrected for ^{17}O and ^{18}O. The predicted minimum total cross section, 0.1013 b, agrees with the experimental value of 0.1028 ± 0.018 b. As shown in Fig. 5, our evaluation fits this "window" data much better than ENDF/B-VI.5. The present evaluation should give more reliable results than ENDF/B-VI.5 for applications that are very sensitive to σ_{total} in the "window" region. Finally, we note the good agreement between predicted and experimental $d\sigma/d\Omega$ values at 2240 keV [MZ62] and 2560 keV [DR76].

Levels 11 and 12. ($5/2^+$), 2889 keV; ($7/2^-$), 3007 keV. Energies and approximate neutron widths of 0.22 keV for level 11 and 0.16 keV for level 12 are based on analysis of the FJF73 σ_{total} data. Their resolution at these energies is better than that of JO74 but inadequate for determination of accurate widths or J^π values. FJF73 point out that J^π is not $1/2^+$ since weak peaks, not dips, in σ_{total} are observed. We assumed $J^\pi = (5/2^+)$ for level 11 and $J^\pi = (7/2^-)$ for level 12 as tentatively assigned by TI93 on the basis of data from the reactions ^{17}O(e, e'), $^{12}C(^6Li, p)^{17}O$, $^{15}N(^3He, p)^{17}O$ and $^{18}O(d, t)^{17}O$.

5.2. $3100 < E_n < 6300$ keV: Narrow Resonances

We discuss in this section our determination of E_r, Γ_n, and Γ_α for 15 narrow resonances. Nine of these resonances are summarized in Table 3, where total widths from the present evaluation are compared with widths given by FJ70, FJF73, and CI80. Energies were determined by fits to the very high resolution σ_{total} data of CI80.

Levels 13, 15, and 16. $5/2^-$, 3211 keV; $5/2^+$, 3438 keV; and $5/2^-$, 3441 keV

Neutron widths, as determined by fits to the σ_{total} data of FJF73, are in good agreement with values quoted by FJ70 and CI80. However, these widths do not give

good fits to the CI80 data near the maxima of these resonances. The CI80 cross sections at the maxima are significantly larger (~15%) than theoretical values based on widths quoted by CI80. The 3438- and 3441-keV peaks are well-resolved in the CI80 data. The discrepancies in peak maxima are not due to variations in the time channel width, Δt_{CH}, since Δt_{CH} is constant over the energy range of interest. However, there can be significant experimental uncertainties associated with measurement of small transmission values. For example, small background errors at transmission minima can produce large errors in σ_{total} maxima . For the thick (1.201 atoms/b) sample of CI80, transmissions at the maxima are about 0.0013, 0.0022, and 0.0007 for levels 13, 15, and 16, respectively. It may be that CI80 used data from a thin sample measurement to determine widths. CI80 normalized their thick sample data to data from a previous thin sample measurement [CI74] having poorer time resolution (0.02 ns/m). Unfortunately, the thin sample data is not available; only a plot is given in Ref [CI74]. However, resonance maxima read from this plot are more consistent with our theoretical values than with the CI80 thick sample data.

Note also that our resonance parameters give differential elastic cross sections in good agreement with the data of FJ70 as shown in Fig 13. Our J^{π} values agree with FJ70, FJF73, and TI93.

Level 18. $7/2^-$, 3767 keV

The neutron width was determined by sequential fits to FJF73, JO74, and CI80 σ_{total} data. Good fits were obtained for the FJF73 and JO74 data, but the CI80 resonance maximum is about 5% higher than our predicted value. As is the case for the 3211, 3438, and 3441 keV resonances, the transmission at the resonance maximum is rather small, about 0.0006 for the CI80 thick sample data. In addition, our predicted maximum for this resonance is consistent with the CI74 thin sample plot.

FJF73 revised their earlier [JF70] angular distribution analysis in the 3767 keV region with the result that a single $7/2^-$ resonance of width 19 keV gave satisfactory fits to the data. We also have good agreement (see Figs. 12 and 14) with the data with a neutron width, $\Gamma_n = 18.5$ keV. The alpha width, $\Gamma_\alpha = 0.026$ keV, was determined by fits to the BH73 data.

Levels 24 - 27. $1/2^+$, 4467 keV; $5/2^+$, 4527 keV; $7/2^+$, 4594 keV; and $5/2^-$, 4631 keV.
Neutron and alpha widths for these levels were determined by sequential fits to CI80 σ_{total} and BH73 $\sigma_{n,\alpha}$ data. Total widths and J^{π} values are in good agreement with values quoted by CI80 and TI93. However, for level 27 our Γ_α of 3.9 keV is significantly larger than the value of 2.0 keV given in TI93. As shown in Fig. 7, the data in this energy region is well represented by the SAMMY fit. The 4467-keV s-wave resonance is responsible for the sharp dip in σ_{total} (Fig. 6) and an isolated peak in $\sigma_{n,\alpha}$ (Fig. 7).

Level 30. $7/2^-$, 5124 keV. Our total width, 26.1 keV, agrees with TI93. The good fit to total and reaction data supports the assignment of J = 7/2 by TI93. Our peak energy, 5124.0 ± 0.3 keV, is significantly smaller than the TI93 value of 5127.0 ± 1.6 keV, which is identical to the value obtained from a resonance analysis by CI80 (see Table 5a). However, CI80 quote 5124.55 ± 0.25 keV in their Table 3. The two CI80 values are clearly inconsistent since the peak is nearly symmetric ($\phi = 1.2^o$).

Level 31. $(1/2^-)$, 5311 keV. On the basis of fits to their (α, α) angular distribution measurements, Kerr, et al. [KMR68] deduced $J^\pi = 1/2-$ and $\Gamma \approx 8$ keV for a level at E_n = 5312 keV. Our fit to the BH73 data with a single $J^\pi = 1/2^-$ level yields $\Gamma_{\mathbf{n}} \approx 0.5$ keV and $\Gamma_\alpha \approx 4$ keV with an upper limit of 8 keV for the total width. Although this weak peak is clearly visible only in the (n, α) data, the fit to the CI80 σ_{total} data does improve slightly upon inclusion of this p-wave resonance. An s-wave dip in σ_{total} at this energy is not consistent with the CI80 data.

Level 32. $5/2^+$, 5369 keV. Our total width of 4.03 keV is consistent with the value 3.75 ± 0.14 keV given by CI80. The good fits to both the total and reaction data support the $5/2^+$ assignment by TI93.

Level 34. $5/2^-$, 5672 keV. This resonance is very weak in σ_{total} but relatively strong in (n, α). TI93 have a level near this energy with $J^\pi = 5/2^-$ and $\Gamma = 16 \pm 1$ keV. We obtain a good fit to the BH73 $\sigma_{n,\alpha}$ data with $\Gamma_\alpha = 15.6$ keV, $\Gamma_{\mathbf{n}} = 0.6$ keV, $\Gamma = 16.2$ keV.

Level 36. $3/2^-$, 5993 keV. On the basis of better fits to σ_{total} and $\sigma_{n,\alpha}$ data, we conclude that $J^\pi = 3/2^-$ rather than $3/2^+$ as given by TI93 and CI80. Our total width is 15.0 keV as compared with 12.4 ± 0.3 keV by CI80. Our peak energy, 5998.9 ± 0.5 keV, is not in agreement with CI80 (5995.68 ± 0.15 keV). Some of this difference is probably due to the large difference in phase shifts between $\mathbf{p_{3/2}}$ ($\phi = 48^o$) and $\mathbf{d_{3/2}}$ ($\phi = 14^o$).

Level 37. $9/2^+$, 6076 keV. We find that $J^\pi = 9/2^+$ gives a much better fit to both the CI80 σ_{total} and BH73 $\sigma_{n,\alpha}$ data than does $J^\pi = (5/2^-)$ as assigned by TI93 and CI80. On the basis of their (α, n) angular distributions, Kerr, et al. [KMR68] assigned $J^\pi = 9/2^+$ although they did not resolve the adjacent, weaker 6087 keV $(1/2^-)$ level. Our total width is 5.64 keV as compared with 4.26 ± 0.24 keV by CI80.

Level 38. $(1/2^-)$, 6087 keV. Poorer fits with J > 1/2 lead us to prefer $J^\pi = 1/2^-$ in agreement with TI93 and CI80. Our total width is 18.0 keV as compared with 17.8 ± 1.8 keV by CI80. The resonant energy for this level is 7 keV less than the peak energy.

5.3. $3100 < E_n < 6300$ keV: Broad Resonances

Level 14, $3/2^+$, 3291 keV; and Level 17, $3/2^-$, 3512 keV. These broad resonances are the primary components of the total cross section for $3200 < E_n < 3700$ keV. Each has a small alpha width whose value is determined by the low-energy (n, α) data. The alpha widths are rather sensitive to the α channel radius.

The 3800-5300 keV region is characterized by several broad overlapping resonances. In companion papers, Johnson [JO73] and Fowler, et al. [FJF73] have reported R-matrix analyses of total [FJF73] and reaction [BH73] cross sections leading to J^π assignments and interference patterns for pairs of $\mathbf{p_{1/2}}$ and $\mathbf{d_{3/2}}$ resonances. Using the more recent CI80 higher-resolution data in addition to the FJF73, BH73, and JO74 data, we have confirmed the J^π assignments and interference signs of JO73. Some of our Γ_n and Γ_α values are quite different from those of JO73 as would be expected since our formalism (Reich-Moore) is different from that of JO73.

Level 19. $1/2^+$, 4061 keV. This s-wave resonance produces a dip in σ_{total} and a peak in $\sigma_{n,\alpha}$ as indicated in Figs. 6 and 7. Both the dip and peak are affected by the presence of the 3990-keV p-wave resonance that populates Level 20.

Levels 20 and 22. $1/2^-$, 3990 and 4312 keV. Acceptable fits to σ_{total}, $\sigma_{n,\alpha}$, and $d\sigma/d\Omega$ can obtained for this p-wave resonance pair only if the sign of the interference term, $\gamma_n\gamma_\gamma$, is negative.

Level 23. $3/2^-$, 4303 keV. At this energy, both σ_{total} and $\sigma_{n,\alpha}$ contain significant contributions from the 4180- and 4312-keV resonances. There is also an s-wave "background" of about 0.4 b in σ_{total}. However, the 4303-keV resonance provides the dominant partial cross section.

Levels 21 and 29. $3/2^+$, 4180 and 5066 keV. Good fits to σ_{total}, $\sigma_{n,\alpha}$, and $d\sigma/d\Omega$ are obtained for the strong 4180-keV resonance. The partial cross section due to this $\mathbf{d_{3/2}}$ pair is quite large for $4200 < E_n < 5000$ keV. We find, as did Johnson (see Figs. 11-12 of JO73) that the sign of the interference term, $\gamma_n\gamma_\gamma$, must be negative in order to fit the total and (n, α) cross sections between these resonances. If $\gamma_n\gamma_\gamma$ is positive, the $\mathbf{d_{3/2}}$ partial cross section between resonances vanishes, and the theory underpredicts the data.

Level 28. $3/2^-$, 4820 keV. This rather asymmetric resonance ($\phi = 39.2^o$) is relatively isolated in σ_{total} but appears on the tail of the 5066 keV $\mathbf{d_{3/2}}$ resonance in $\sigma_{n,\alpha}$. There is a large difference in our peak energy, 4839.1 ± 1.5 keV, and the CI80 value of 4829.0 ± 0.4 keV. Our total width, 61.1 keV, is consistent with CI80 (58.8 keV).

Level 33. $3/2^-$, 5575 keV. Good fits to both the JO74 and CI80 σ_{total} data were obtained for this broad $\mathbf{p_{3/2}}$ resonance. The peak asymmetry is reduced owing to interference with the 5993 keV $\mathbf{p_{3/2}}$ resonance. Our peak energy, 5637 keV, agrees with the value given by Johnson [JO73]. CI80 do not report an energy or width for this level.

Level 35. $7/2^+$, 5919 keV. This level is well separated from its neighbors, and the fit for $\mathbf{g_{7/2}}$ is excellent. Our peak energy, 5919.1 ± 0.5 keV, is consistent with the value of 5919.67 ± 0.14 keV quoted by CI80. Our total width is 24.7 keV as compared with 24.6 ± 0.3 keV by CI80.

Level 39. $5/2^+$, 6208 keV. A broad resonance with large Γ_α and small $\Gamma_\mathbf{n}$ is required to fit the BH73 reaction data and the CI80 σ_{total} data for $6100 < E_n < 6300$ keV.

5.4. Thermal and Integral Quantities

Total and capture cross sections for $E_n = 0.0253$ eV and $T = 300^oK$ are in good agreement with the ENDF/B-VI.5 values as shown in the following tabulation.

Cross Section	ENDF/B-VI.5	Present Evaluation	Ratio
Total	4.0138 b	4.0297 b	1.004
Capture	0.190 mb	0.196 mb	1.032

We used the experimental radiation width, 2.7 ± 0.5 eV, for the 434 keV resonance and $\Gamma_\gamma = 0.25$ eV for all other resonances to compute the resonance capture integral, I_γ. Our value, $I_\gamma = 0.24$ mb, is in good agreement with the value of 0.27 ± 0.03 mb given by Mughabghab and Garber [MU73] but is significantly lower than the more recent value of 0.36 mb given by Mughabghab, et al. [MU81].

5.5 Integral Test: Thermal Reactor Benchmarks

Point-wise cross sections generated from our Reich-Moore resonance parameter representation were used for five thermal reactor benchmarks [FO58] consisting of three reflected and two bare spheres of highly enriched uranium as aqueous solutions of uranyl fluoride. These benchmarks are useful for testing fast scattering by H_2O as well as ^{235}U fission and capture in the thermal range. Calculated multiplication factors, k_{eff}, were obtained with the BONAMI-NITAWL-XSDRNPM sequence of the SCALE-4.3 system [SC95] using the 199-group VITAMIN-B6 cross section data library [WH95], which is based on the ENDF/B-VI.5 evaluation. As indicated in the following table, the k_{eff} values based on the present evaluation are in excellent agreement with k_{eff} values computed with ENDF/B-VI.5 point-wise cross sections. The largest $|\Delta k_{eff}|$ value is 0.0012.

Benchmark	ENDF/B-VI.5	Present Evaluation	Δk_{eff}
L-7	1.0006	0.9995	-0.0011
L-8	1.0050	1.0047	-0.0003
L-9	1.0020	1.0021	0.0001
L-10	0.9986	0.9974	-0.0012
L-11	0.9997	0.9996	-0.0001

5.6 Integral Calculation of Neutron Flux for Broomstick Experiment

Point-wise cross section values based on our resonance parameter representation have been used to compute transmitted neutron flux for comparison with the "broomstick" experiment [MA72]. This experiment was designed to test neutron total cross sections for oxygen in the 2 - 8 MeV range. The liquid oxygen sample was a cylinder approximately 10 cm in diameter located so that its axis was coincident with the axis of the neutron beam produced by the ORNL Tower Shielding Reactor. Fig. 16 shows the variation with energy of the experimental flux and calculated flux based on point-wise cross sections from ENDF/B-VI.5 and the present evaluation. The error bars include a 10% contribution due to power calibration uncertainties. Calculated values were broadened to account for the detector resolution and corrected for fine structure in the incident beam due to passage through 5 cm of water. Unfortunately, the fine structure corrections may be subject to sizeable error since the corrections were based on out-of-date total cross sections. Both calculations reproduce the general trend of the data. Where the flux is very small (4-7 MeV), ENDF/B-VI.5 gives slightly better agreement with experiment although the difference in the two evaluations is of the order of the experimental uncertainties. In the region of peak flux, the present evaluation gives somewhat better agreement with experiment. However, difficulties in the unfolding of the experimental data and possible error in the incident beam fine structure corrections preclude more definite conclusions about the quality of agreement of experimental and calculated flux values.

6. Summary and Conclusions

We have evaluated ^{16}O neutron cross sections in the resolved resonance region with the multilevel Reich-Moore R-matrix formalism. In order to give a proper treatment for the alpha particle exit channel, an algorithm to calculate charged particle penetrabilities and shifts was incorporated in the SAMMY code. When uncertainties are taken into account, there is good agreement between theory and experiment for ^{16}O total, reaction, and differential elastic cross sections up to E_n = 6300 keV. New J^π assignments have been proposed for levels with E_r = 5993 keV [3/2-] and 6076 keV [9/2+].

Point-wise cross section values generated from our Reich-Moore resonance parameter representation have been used for several thermal reactor benchmark calculations. The k_{eff} values based on the present evaluation are in excellent agreement with values computed using ENDF/B-VI.5 point-wise cross sections. Thermal values of total and capture cross sections agree well with the corresponding ENDF/B-VI.5 values. For the "broomstick" experiment, our calculated values at the peak of transmitted flux, 2.2 to 2.5 MeV, are in somewhat better agreement with the data than ENDF/B-VI.5 values. Our evaluation fits the 2.35 MeV "window" data much better than does ENDF/B-VI.5.

The present Reich-Moore resonance parameter evaluation gives an accurate, few-parameter representation of the ^{16}O neutron cross section data. This representation should prove to be extremely useful for radiation transport calculations that are utilized for criticality safety applications. For applications that are sensitive to σ_{total} in the 2.35 MeV "window" region, the present evaluation should give more reliable results than ENDF/B-VI.5.

Inclusion of resonance parameters for outgoing charged particle channels would require modification of cross section processing codes such as AMPX and NJOY. In addition, a revision to the ENDF format will be proposed to accommodate this new feature.

Acknowledgements

We are pleased to acknowledge illuminating discussions with Drs. K. Guber, H. Derrien, D. C. Larson, J. A. Harvey, R. W. Roussin, C. Y. Fu, D. T. Ingersoll, C. Lubitz, and J. C. Nimal. We are indebted to Dr. G. M. Hale for providing us with the 2.35 MeV window data of JO80 corrected for ^{17}O and ^{18}O. We thank Dr. M. Jaeger for sending us the (α, n) data of Drotleff, et al. [DR93] and Dr. C. Raepsaet for sending us some preliminary comparisons of different ^{16}O evaluations [RA00].

References

AB64. M. Abramowitz, NBS Handbook of Mathematical Functions, p. 537 (1964).

BA81. A. R. Barnett, Comp. Phys. Comm. **27**, 147 (1982); Comp. Phys. Comm. **21**, 297 (1981).

BH73. J. K. Bair and F. X. Haas, Phys. Rev. **C7**, 1356 (1973).

BL51. I. Block, et al., Rev. Mod. Phys 23, 147 (1951).

CA98. E. Caro, "^{16}O Neutron Cross Section Evaluation", Proc. Intl. Conf. On the Physics of Nucl. Science and Technology, Long Island, N. Y., October, 1998.

CI74. S. Cierjacks, in *Nuclear Structure Studies with Neutrons*, eds. J. Ero and J. Szucs, Plenum Press, London, 1974, p. 299..

CI80. S. Cierjacks, F. Hinterberger, G. Schmalz, D. Erbe, P. B Rossen, and B. Leugers, "Nucl. Inst. Meth. **169** (1980) 185.

DR76. L. Drigo, G. Tornielli, and G. Zannoni, Nuovo Cimento **31A**, N.1, 1 (1976).

DR93. H. W. Drotleff, A. Denker, H. Knee, M. Soine, G. Wolf, J. W. Hammer, U. Greife, C. Rolfs, and H.P. Trautvetter, Astrophys. J. **414**, 735 (1993).

FC58. J. L. Fowler and H. O. Cohn, Phys. Rev. **109**, 89 (1958).

FJ70. J. L. Fowler and C. H. Johnson, Phys. Rev. **C2**, 124 (1970).

FJF73. J. L. Fowler, C. H. Johnson, and R. M. Feezel, Phys. Rev. **C8**, 545 (1973).

FO58. J. K. Fox, et al., "Critical Parameters of Uranium Soluitons in Simple Geometry," ORNL-2609, 42 (1958).

GR92. N. M. Greene, W. E. Ford, III, L. M. Petrie, and J. W. Arwood, "AMPX-77 A Modular Code System for Generating Coupled Multigroup Neutron Gamma Cross Section Libraries from ENDF/B-IV and/or ENDF/B-V," ORNL/CSD/TM-283 (October 1992).

HA91. G. M. Hale, P. G. Young, M. Chadwick, and Z. P. Chen, Proc. Int. Conf. On Nuclear Data for Science and Technology, Julich, Germany, 1991.

HH62. W. Hunzinger and P. Huber, Helv. Phys. Acta. **35**, 351 (1962).

JF67. C. H. Johnson and J. L. Fowler, Phys. Rev. **162**, 890 (1967).

JO73. C. H. Johnson, Phys. Rev. **C7**, 561 (1973).

JO74. C. H. Johnson, J. L. Fowler, L. A. Galloway, and N. W. Hill, Oak Ridge National Laboratory Report ORNL-4937 (1974).

JO80. C. H. Johnson, J. L. Fowler, N. W. Hill, and J. M. Ortolf, Proc. Int. Conf. On Nuclear Cross Sections for Technology, Knoxville, p. 807 (1980).

KMR68. G. W. Kerr, J. M. Morris, and J. R. Risser, Nucl. Phys. **A110**, 637 (1968).

KP72. W. Kinney and F. G. Perey, Oak Ridge National Laboratory Report ORNL-4780, 1972.

LA80. D. C. Larson, Symposium on Neturon Cross Sections from 10 to 50 MeV, BNL-NCS-51245, p. 277 (1980); D. C. Larson, J. A. Harver, and N. W. Hill, Proc. Int. Conf. On Nuclear Cross Sections for Technology, Knoxville, p. 34 (1980).

LA98. N. M. Larson, Oak Ridge National Laboratory Report ORNL/TM-9179/R4, 1998.

LE98. L. C. Leal, R. O. Sayer, N. M. Larson, and R. R. Spencer, "R-Matrix Evaluation of ^{16}O Neutron Cross Sections up to 6.3 MeV," ANS Winter Meeting, Washington, D. C., Nov. 16-20, 1998.

LS66. D. Lister and A. Sayres, Physical Review **143**, 745 (1966).

LT58. A. M. Lane and R. G. Thomas, Rev. Mod. Phys 30, 257 (1958).

MA87. D. M. Manley, et al., Phys. Rev. C36, 1700 (1987).

MA94. R. E. MacFarlane and D. W. Muir, "The NJOY Nuclear Data Processing System Version 91," LA-12740-M, 1994.

MZ62. J. P. Martin and M. S. Zucker, Bull. Appl. Phys. **7**, 72 (1962).

MU73. S. F. Mughabghab and D. I. Garber, BNL 325, 1973.

MU81. S. F. Mughabghab, M. Divadeenam, and N. E. Holden, *Neutron Cross Sections*, Vol. 1, Part A, Academic Press, Inc. (1981).

OH84. M. Ohkubo, private communication to NNDC, BNL (1984).

OK55. A. Okazaki, Phys. Rev. **99**, 55 (1955).

PH60. D. D. Phillips, WASH-1028, 29 (1960).

RA00. C. Raepsaet, "Preliminary Comparison Between Different Evaluations of 8-O-16," CEA Report SERMA/LEPP/RT/00-2738/A, 2000.

SA00. R. O. Sayer, Oak Ridge National Laboratory Report, to be published.

SC77. I. Schouky, et al., KFK-2503, 1977.

SC95. S*CALE: A Modular Code System for Performing Standardized Computer Analyses for Licensing Evaluation*, NUREG/CR-0200, Rev. 4 (ORNL/NUREG/CSD-2R4), Vols. I, II, and III (April 1995). Available from Radiation Safety Information Computational Center at Oak Ridge National Laboratory as CCC-545.

SE67. K. K. Sekharan, A. S. Divatia, M. K. Mehta, S. S. Kerekatte, and K. B. Nambiar, Phys. Rev. 156, 1187 (1967).

TI93. D. R. Tilley, et al., Nucl. Phys. **A564**, 1 (1993).

WCB57. R. B. Walton, J. D. Clement, and F. Boreli, Phys. Rev. **107**, 1065 (1957).

WH95. J. E. White, R. Q. Wright, D. T. Ingersoll, R. W. Roussin, N. M. Greene, and R. E. MacFarlane, "VITAMIN-B6: A Fine-Group Cross Section Library Based on ENDF/B-VI for Radiation Transport Applications," pp. 733-36 in *Nuclear Data for Science and Technology*, *Proc. Of the International Conference*, ed. J. K. Dickens, Oak Ridge National Laboratory, 1995. See also D. T. Ingersoll, et al., *Production and Testing of the VITAMIN-B6 FineGroup and the BUGLE-93 Broad-Group Neutron/Photon Cross-Section Libraries Derived from ENDF/B-VI Nuclear Data*, NUREG/CR-6214 (ORNL-6795), U. S. Nuclear Regulatory Commission, January, 1995.

Appendix. Computation of Charged Particle Penetrabilities

PSPHICOUL is a routine for computation of Coulomb penetrability P, shift S, and phase ϕ as a function of incident neutron laboratory energy E_n for the reaction $n + A_2 \rightarrow A_3 + A_4$. A slightly modified version of the routine COULFG of Barnett [BA81] is used to compute the Coulomb wave functions and their derivatives. PSPHICOUL has been adapted for use in SAMMY [LA98].

Input quantities for PSPHICOUL are charges, masses, reaction Q value, channel radius a_c, E_n(min), E_n(max), E_n(increment). Quantities computed are E_n, k, ρ, η, and P_0, ..., P_4, where

$$\eta = 4\pi^2 Z_3 Z_4 e^2 M / h^2 k$$

$$k = 2\pi [2 M (E_{cm} - Q)]^{0.5} / h$$

$$\rho = k a_c$$

$$M = A_3 A_4 / (A_3 + A_4)$$

$$P_L = \rho / (F_L^2 + G_L^2) = \text{penetrability for angular momentum L}$$

F_L and G_L are the regular and irregular Coulomb wave functions, respectively, as defined by Lane and Thomas [LT58] for example. The shift and phase are computed from:

$$S_L = (\rho / A_L) \, d A_L / d\rho$$

and

$$\cos \phi_L = G_L / A_L$$

where

$$A_L^2 = F_L^2 + G_L^2$$

The code has been tested against the published F_0, G_0, F'_0, and G'_0 values of Abramowitz [AB64] for the range $0.5 < \eta < 10$; $1 < \rho < 5$. For $\eta < 6.5$ ($F_0 > 10^{-6}$), the region of practical interest for nuclear reactions, the agreement for F_0, G_0, and P_0 is better than 1 part in 10^4. For $0.5 \le \eta \le 6.5$, the agreement for S_0 is better than 4 parts in 10^4. However, note that for $\eta \le 0.5$, $|S_0| \le 0.2$.

Calculated values for L = 1, 2, 3, 4 are in good agreement with the tabulated values of Bloch, et al. [BL51]. The correct asymptotic behavior is exhibited as $\eta \rightarrow 0$: $P_0 \rightarrow \rho$; $S_0 \rightarrow 0$; and $\phi_0 \rightarrow \rho$.

Table 1. Total and Reaction Cross Section Data Sets for ^{16}O Evaluation

Type	Authors	Facility (Flight path)	Energy Analysis Range (MeV)	Atoms/barn	Normalization*
Total	Johnson, et al [JO74]	ORELA 198.731 m	0.2 – 6.3	0.183	(1.000)
Total	Larson [LA80]	ORELA 79.46 m	2.0 – 6.3	0.5485	0.9998
Total	Cierjacks, et al [CI80]	KFK cyclotron 189.25 m	3.14 – 6.3	1.201	0.9663
Total	Fowler, Johnson, and Feezel [FJF73]	ORNL Van de Graaff 41 and 47 m	0.6 – 4.3	0.488	0.9997
Total (2.35 MeV)	Johnson, et al [JO80]	ORELA 198.731 m	2.25 – 2.49	6.7	
(n, α) [from (α,n)]	Bair and Haas [BH73]	ORNL Van de Graaff	3.2 – 6.3		
(n, α) [from (α,n)]	Drotleff, et al [DR93]	Stuttgart Dynamitron	2.87 – 3.48		

***** Normalization obtained by integrating the total cross section from 3.45 to 3.72 MeV.

Table 2. Angular Distribution Data Sets for ^{16}O Cross Section Evaluation

Authors	Facility	Energies (MeV)	FWHM ΔE (keV)	CM Angles (degrees)
Okazaki 1955	University of Wisconsin	.410 – .493	16	46 - 133
Fowler and Cohn 1958	ORNL Van de Graaff	0.73 – 2.15	50	32 - 138
Phillips 1960	LANL	3.0 – 6.0	30	22 - 152
Martin and Zucker 1962	BNL	1.51 – 2.25	33 - 63	21 - 166
Hunzinger and Huber 1962	University of Basel Cockcroft-Walton	2.00 – 4.11	10 – 51	41 - 147
Lister and Sayres 1966	Columbia University Van de Graaff	3.1 – 4.7	18 - 25	Legendre Coefficients
Johnson and Fowler 1967	ORNL Van de Graaff	3.266 – 4.200	14 - 33	20 - 147
Fowler and Johnson 1970	ORNL Van de Graaff	1.833 – 3.441	5 – 13	20 - 146
Kinney and Perey 1972	ORNL Van de Graaff	4.34 – 6.44	60 – 80	16 - 139
L. Drigo, et al. 1976	Lignaro Van de Graaff	2.56, 2.76	30	26 - 156

Table 3. Total Widths for Selected Narrow Resonances in ^{16}O (n, x)

Γ_γ = 0.25 eV for all resonances

J^π	E_r (keV)	Total Width (keV)			
		Fowler and Johnson [FJ70]	Fowler, Johnson, and Feezel [FJF73]	Cierjacks, et al. [CI80]	Present Evaluation
$5/2^-$	3211.76	1.4		1.45	1.51
$5/2^+$	3438.80	0.5		0.68	0.62
$5/2^-$	3441.55	1.1		1.02	1.31
$7/2^-$	3767.00		18.	15.4	18.6
$5/2^+$	4527.36			6.56	5.85
$7/2^+$	4594.83			2.26	1.83
$5/2^-$	4631.21			7.33	7.08
$5/2^+$	5369.27			3.75	4.03
$9/2^+$ *	6076.19			4.26	5.64

* CI80 assigns **$5/2^-$** to the 6076 keV resonance.

Table 4. Energies and Widths for Resonances in ^{16}O (n, x)

Level	J^{π}	$E_X(^{17}O)$ (keV)	E_{peak} (keV)	E_r (keV)	Γ_n (keV)	Γ_α ** (keV)
1	1/2+			-12010.00	9075.00	----
2	1/2+			-4469.10	5410.00	----
3	3/2-	4551.9 ± 1.5	434.60	434.31	44.41	----
4	3/2+	5084.2 ± 2.5	999.30	1000.22	100.36	----
5	3/2-	5375.1 ± 2.0	1312.70	1309.38	43.43	----
6	7/2-	5696.7 ± 2.0	1651.38	1651.38	4.10	----
7	(5/2-)	5732.3 ± 1.9	1689.15	1689.10	0.27	----
8	3/2+	5868.7 ± 2.0	1834.18	1834.09	7.79	----
9	1/2-	5932.0 ± 2.3	1905.78	1901.44	33.50	----
10	1/2+	6380.2 ± 3.3	2351.09	2377.88	162.37	----
11	(5/2+)	6860.7 ± 2.0	2888.87	2888.70	0.22	----
12	(7/2-)	6971.9 ± 2.0	3007.08	3006.90	0.16	----
13	5/2-	7164.6 ± 0.4	3211.76	3211.76	1.50	0.009
14	3/2+	7239.1 ± 8.0	3299.68	3291.01	339.63	0.17
15	5/2+	7378.2 ± 0.4	3438.83	3438.80	0.60	0.020
16	5/2-	7380.8 ± 0.4	3441.56	3441.55	1.30	0.007
17	3/2-	7446.9 ±20.0	3654.25	3511.91	660.21	0.026
18	7/2-	7686.9 ± 0.4	3767.08	3767.00	18.53	0.026
19	1/2+	7963.3 ± 2.2	4062.70	4060.82	105.58	5.23
20	1/2-	7896.3 ± 6.0	4059.82	3989.64	276.19	19.15
21	3/2+	8075.4 ± 2.1	4187.67	4180.04	92.38	9.80
22	1/2-	8199.3 ± 4.5	4327.90	4311.70	43.52	- 0.44
23	3/2-	8190.9 ± 2.5	4321.36	4302.79	54.30	5.77
24	1/2+	8345.7 ± 0.6	4469.48	4467.36	16.89	3.72
25	5/2+	8402.2 ± 0.2	4527.78	4527.36	4.99	0.86
26	7/2+	8465.6 ± 0.2	4594.83	4594.83	1.39	0.44
27	5/2-	8499.8 ± 0.3	4631.26	4631.21	3.20	3.88
28	3/2-	8677.7 ± 1.5	4839.10	4820.33	58.40	2.74
29	3/2+	8909.1 ± 4.0	5087.80	5066.30	94.50	- 34.36
30	7/2-	8963.2 ± 0.5	5123.98	5123.74	23.35	2.75

Γ_γ = 2.7 eV for 434 keV resonance; Γ_γ = 0.25 eV for all other resonances

**** Minus sign means the reduced amplitude product $\gamma_n\gamma_\gamma$ is negative**

$E_X = 4143.36 \text{ keV} + E_r * A_{O16}/(A_{O16} + A_n)$

Table 4, cont. Energies and Widths for Resonances in ^{16}O (n, x)

Level	J^{π}	$E_X(^{17}O)$ (keV)	E_{peak} (keV)	E_r (keV)	Γ_n (keV)	Γ_α ** (keV)
31 a)	(1/2-)	9139.3 ± 6.0	5312.80	5311.00	≈ 0.50	≈ 4.00
32	5/2+	9194.1 ± 0.4	5369.72	5369.27	2.78	1.25
33 b)	3/2-	9387.5 ±14.0	5637.20	5574.84	191.17	0.42
34	5/2-	9479.5 ± 4.1	5672.84	5672.62	0.59	15.63
35	7/2+	9710.9 ± 0.5	5919.05	5918.63	20.50	4.19
36	3/2- *	9781.1 ± 0.5	5998.90	5993.29	14.78	- 0.21
37	9/2+ *	9859.1 ± 0.2	6076.20	6076.19	3.13	2.51
38	(1/2-)	9869.7 ± 0.8	6094.20	6087.44	16.04	1.92
39	5/2+	9983.0	6220.60	6207.95	4.97	109.23
40	7/2+	10100.0	6343.10	6332.24	3.40	181.48
41	(7/2-)	10164.0	6402.00	6400.26	26.54	29.38
42	3/2+ *	10331.2	6602.25	6578.03	90.64	87.94
43	5/2-	10420.3	6673.19	6672.73	1.86	19.06
44	5/2+	10526.9	6824.90	6786.12	10.57	232.54
45	(7/2-)	10554.2	6816.27	6815.17	18.94	28.36
46	7/2-	10886.8	7175.09	7168.68	129.69	223.85
47	(5/2+)	10914.7	7202.83	7198.37	7.86	19.70
48	1/2-	11004.9	7318.38	7294.22	26.16	5.39
49	1/2-	11079.3	7374.79	7373.31	1.89	----
50	3/2-			11131.72	15115.00	----
51	1/2-			19026.72	25755.00	----
52	3/2+			17223.85	772.36	----

$\Gamma_\gamma = 2.7$ eV for 434 keV resonance; $\Gamma_\gamma = 0.25$ eV for all other resonances

* TI93 assigns 3/2+, (5/2-), (5/2+,7/2-), respectively, to Levels 36, 37, 42. See discussion in text.

**** Minus sign means the reduced amplitude product $\gamma_n\gamma_\gamma$ is negative**

$E_X = 4143.36 \text{ keV} + E_r * A_{O16}/(A_{O16} + A_n)$

a) This resonance does not appear in TI93.

b) TI93 : $E_r = 5610$ keV, $\Gamma = 120$ keV; $J^{\pi} = 3/2-$

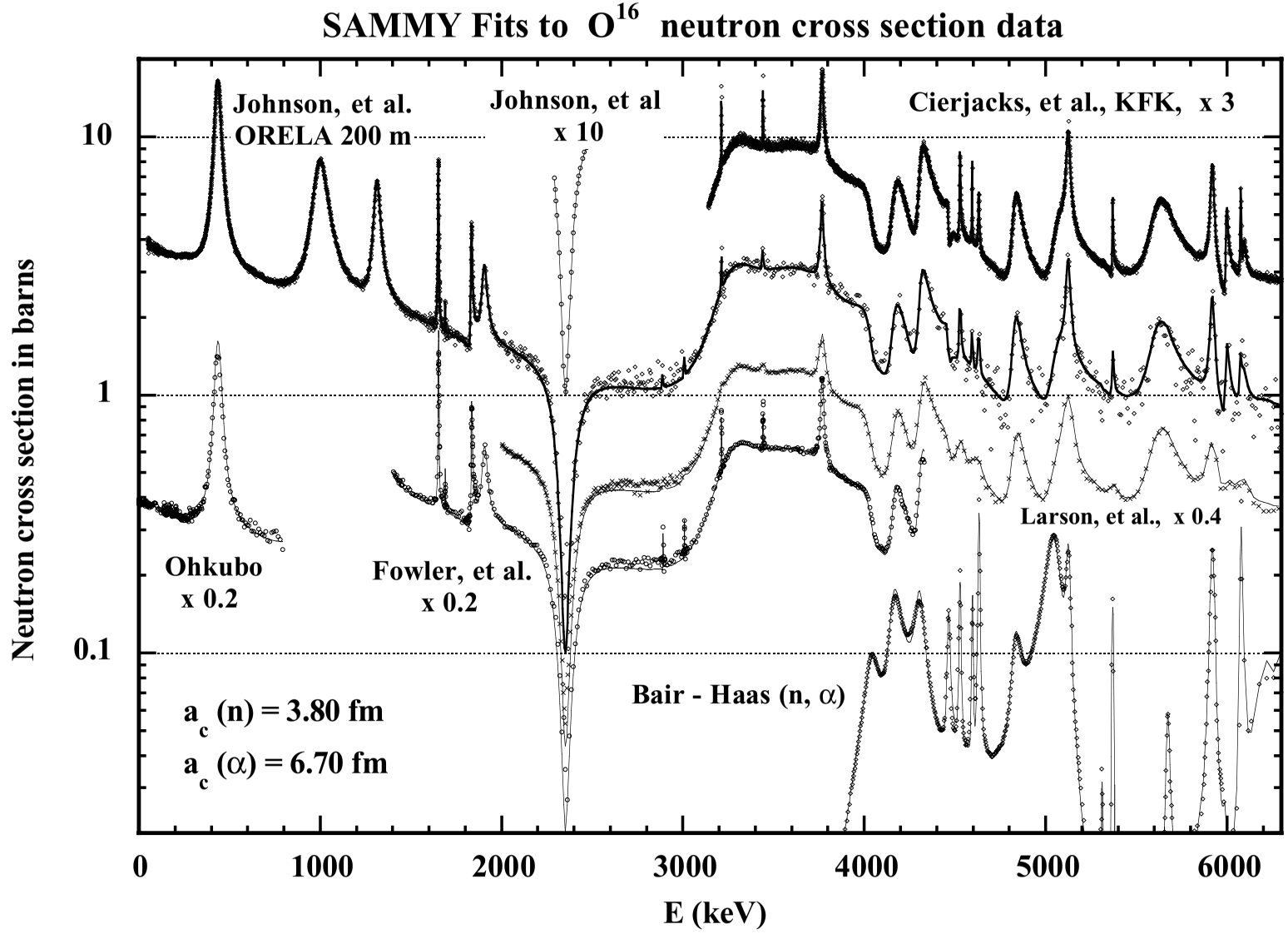

Fig. 1. Comparison of SAMMY predictions to ^{16}O total and reaction cross section data.

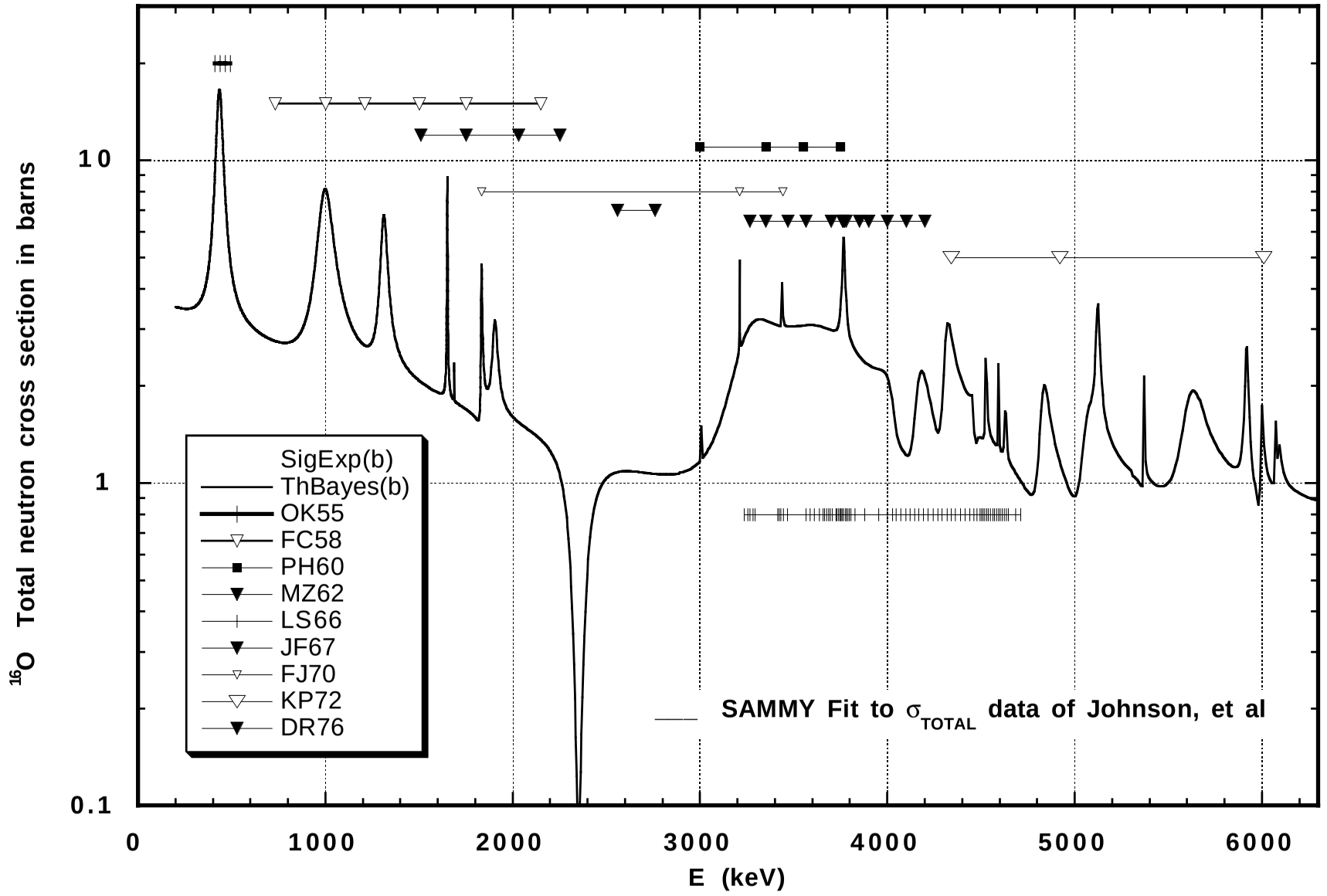

Fig. 2. Neutron energies for which differential elastic ^{16}O data have been evaluated. The curve is the SAMMY fit to the total neutron cross section data of Johnson, et al. [JO74].

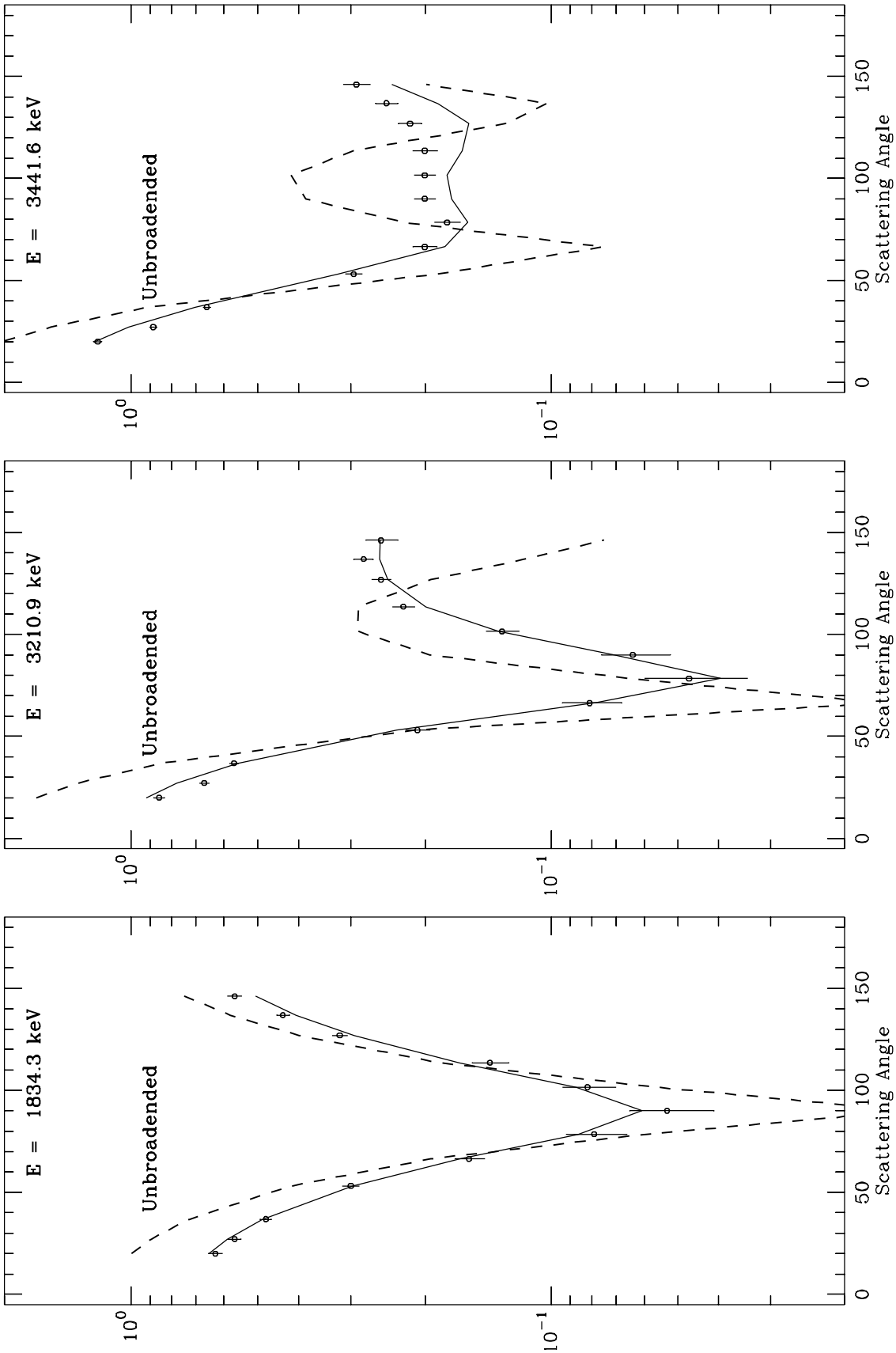

Figure 3. Broadened (solid lines) and unbroadened (dashed lines) SAMMY predictions for differential elastic data (points) of Fowler and Johnson [FJ70].

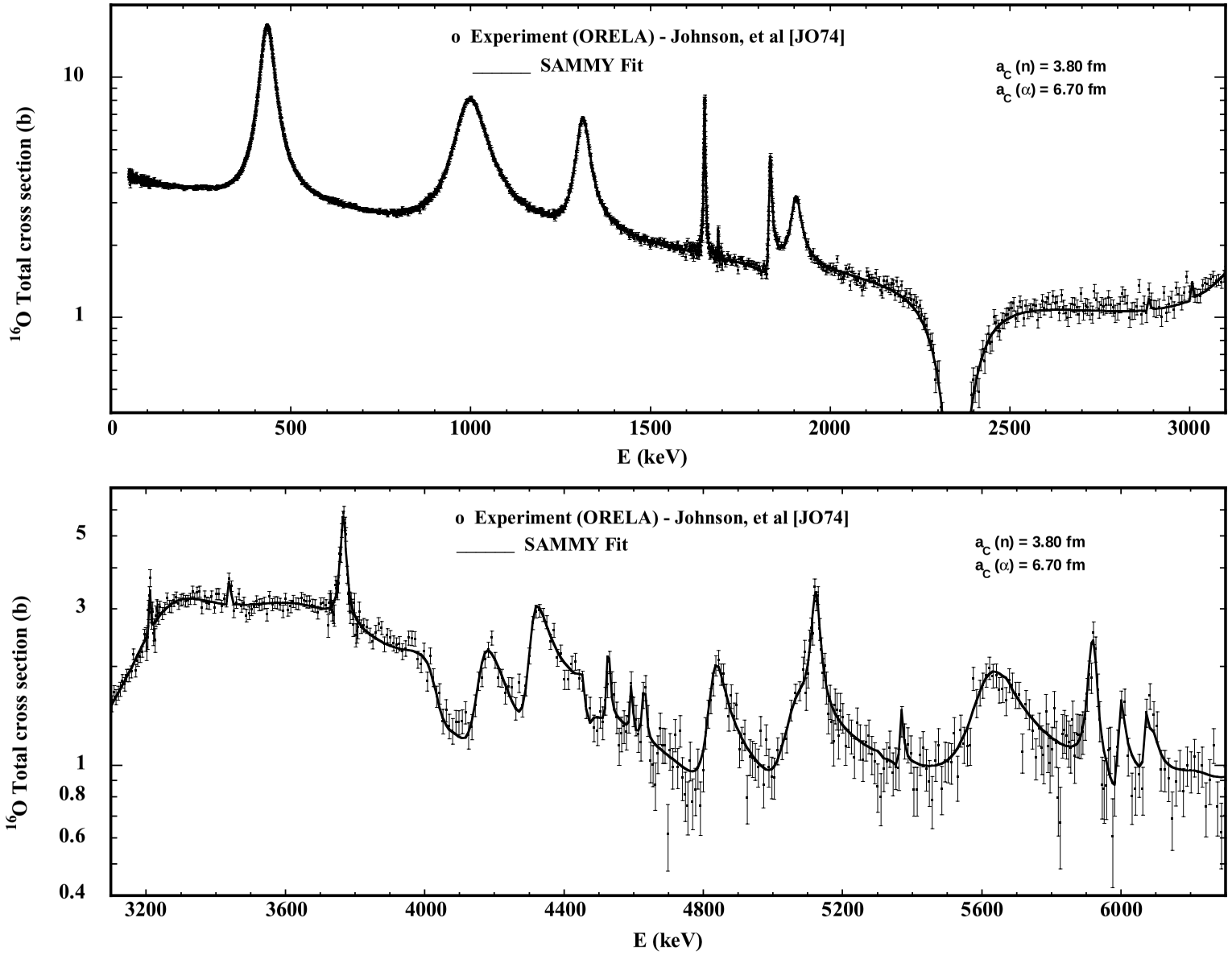

Fig. 4. Comparison of SAMMY predictions to total cross section data of Johnson, et al. [JO74].

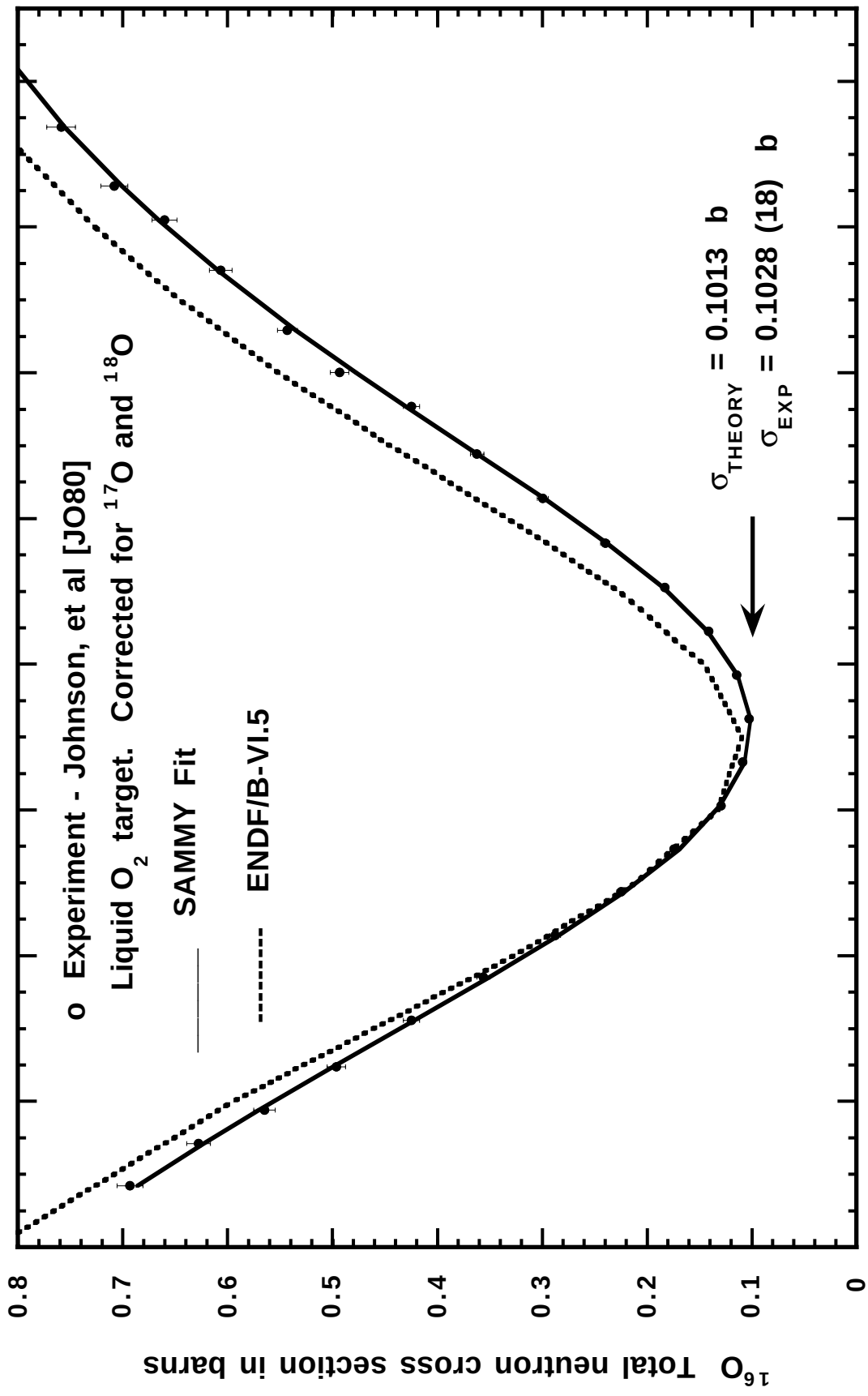

Fig. 5. Comparison of total cross section predictions to ENDF/B-VI.5 and data of Johnson, et al. [JO80].

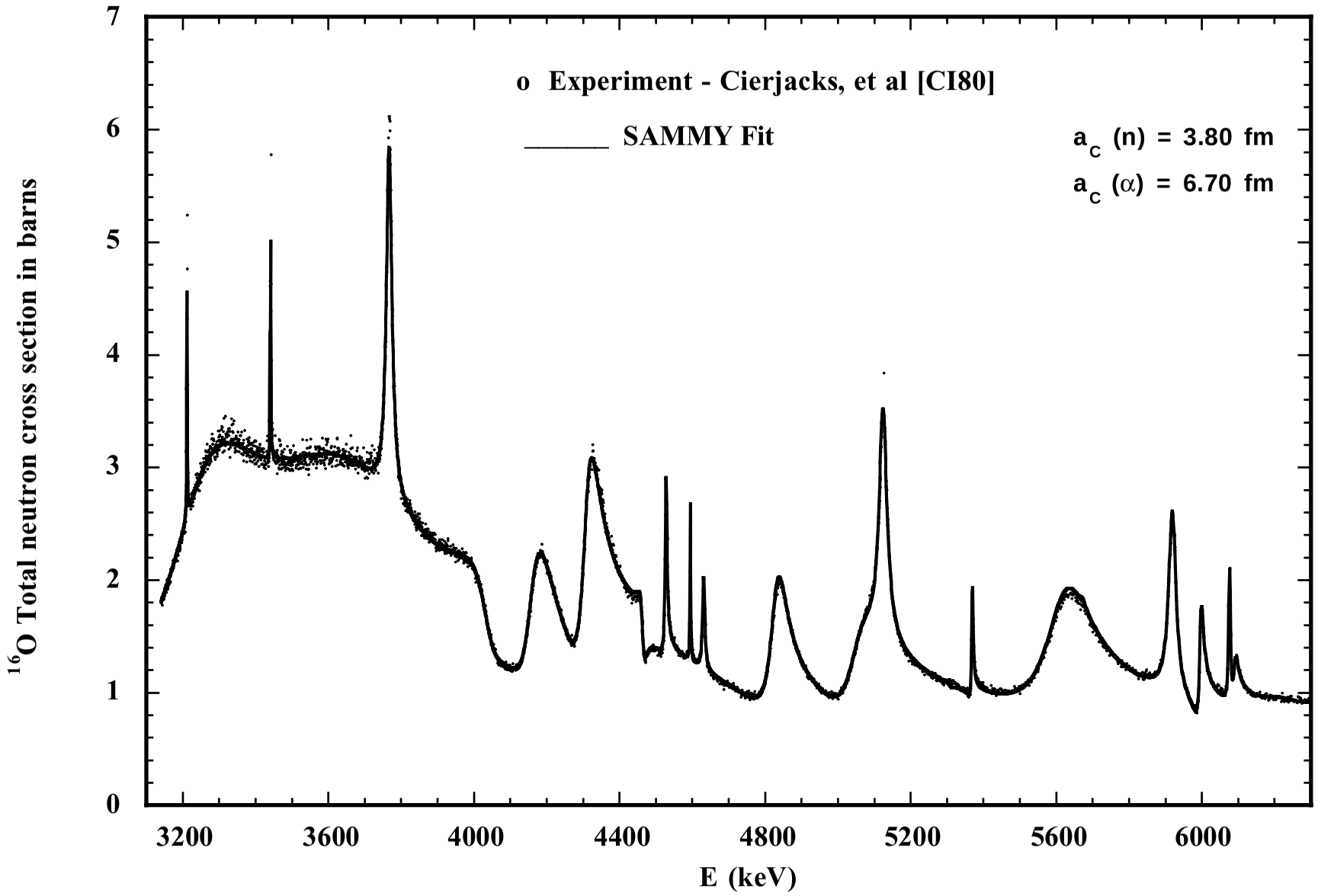

Fig. 6. Comparison of SAMMY predictions to total cross section data of Cierjacks, et al. [CI80].

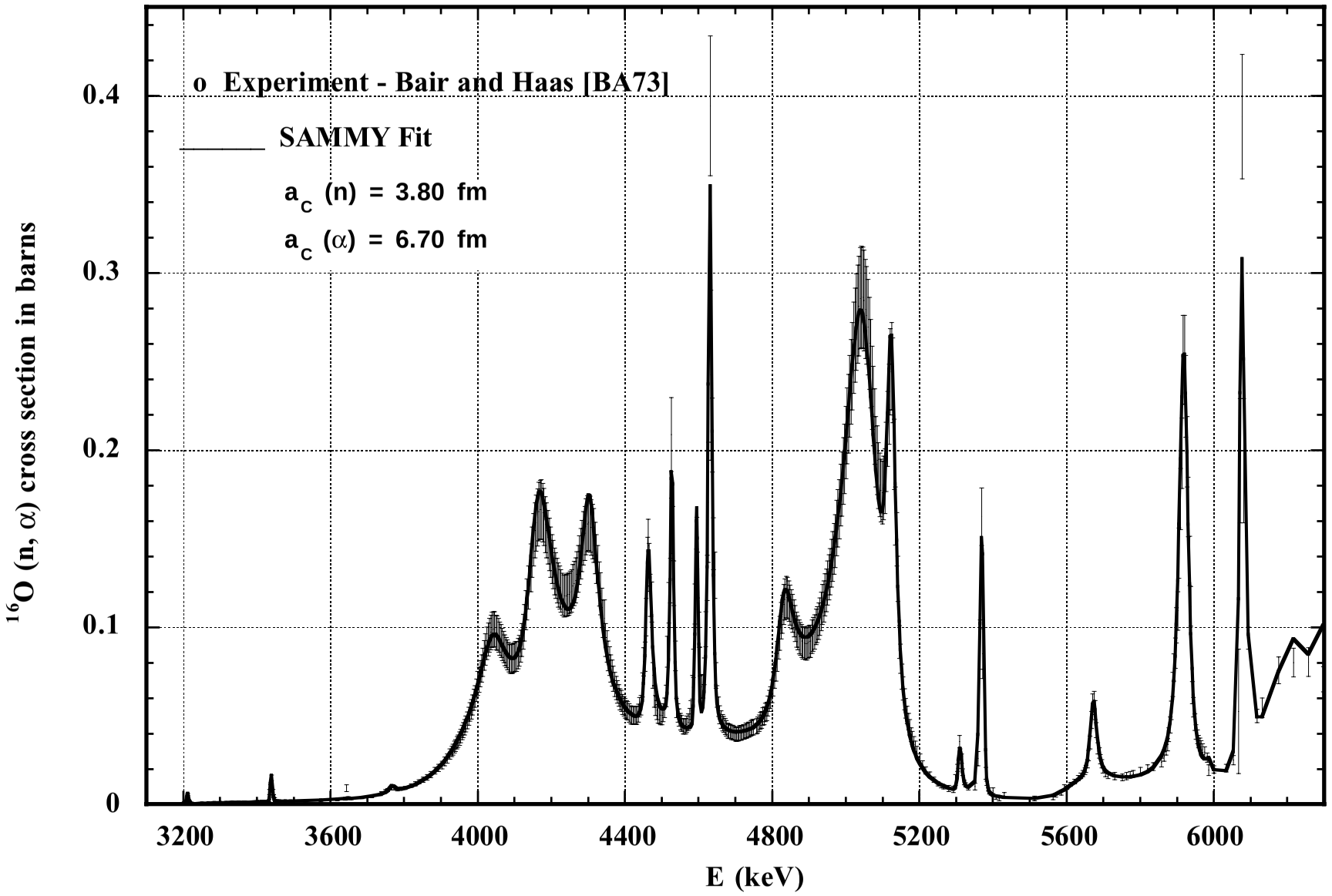

Fig. 7. Comparison of SAMMY predictions to reaction cross section data of Bair and Haas [BH73].

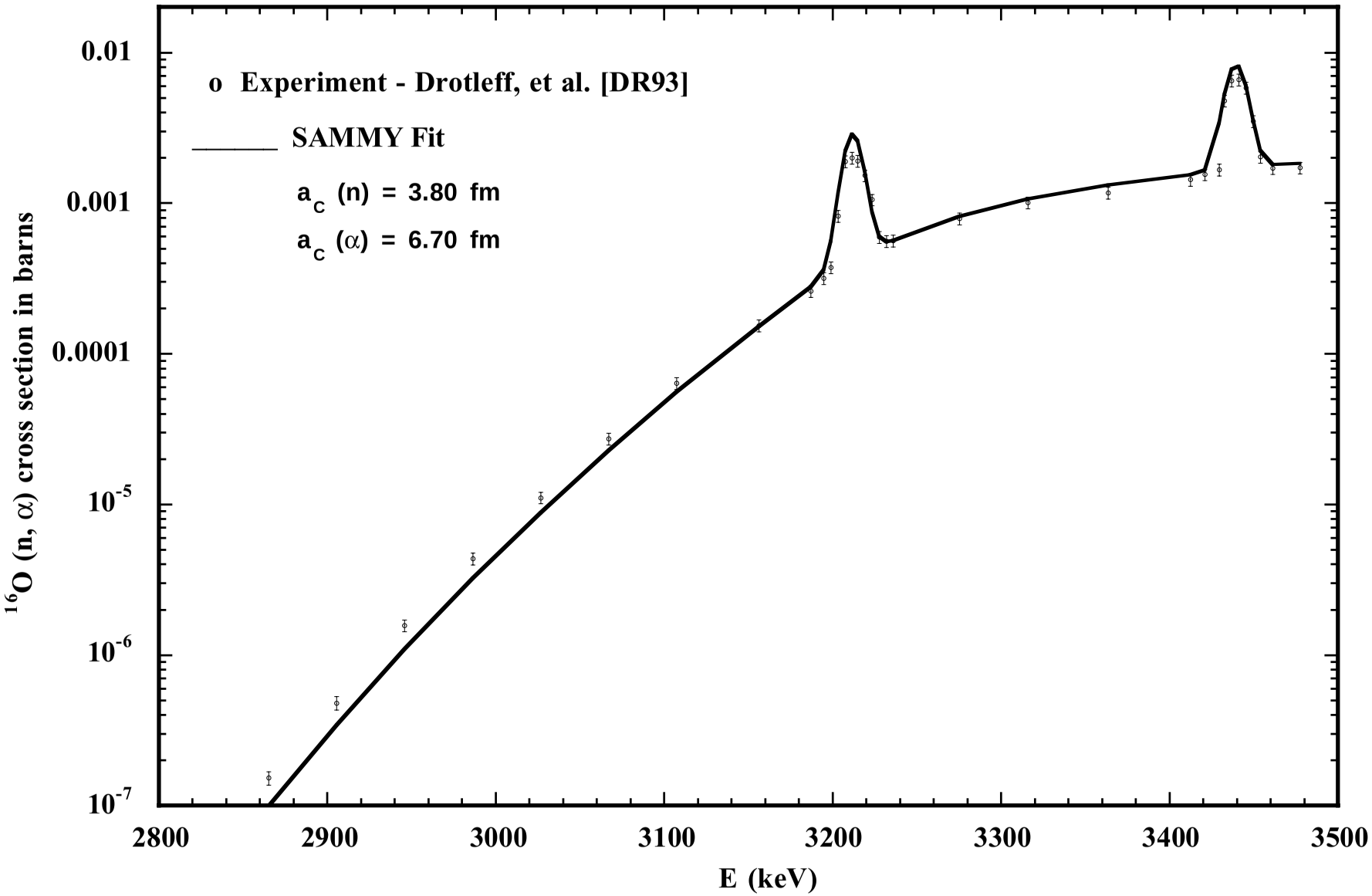

Fig. 8. Comparison of SAMMY predictions to reaction cross section data of Drotleff, et al. [DR93].

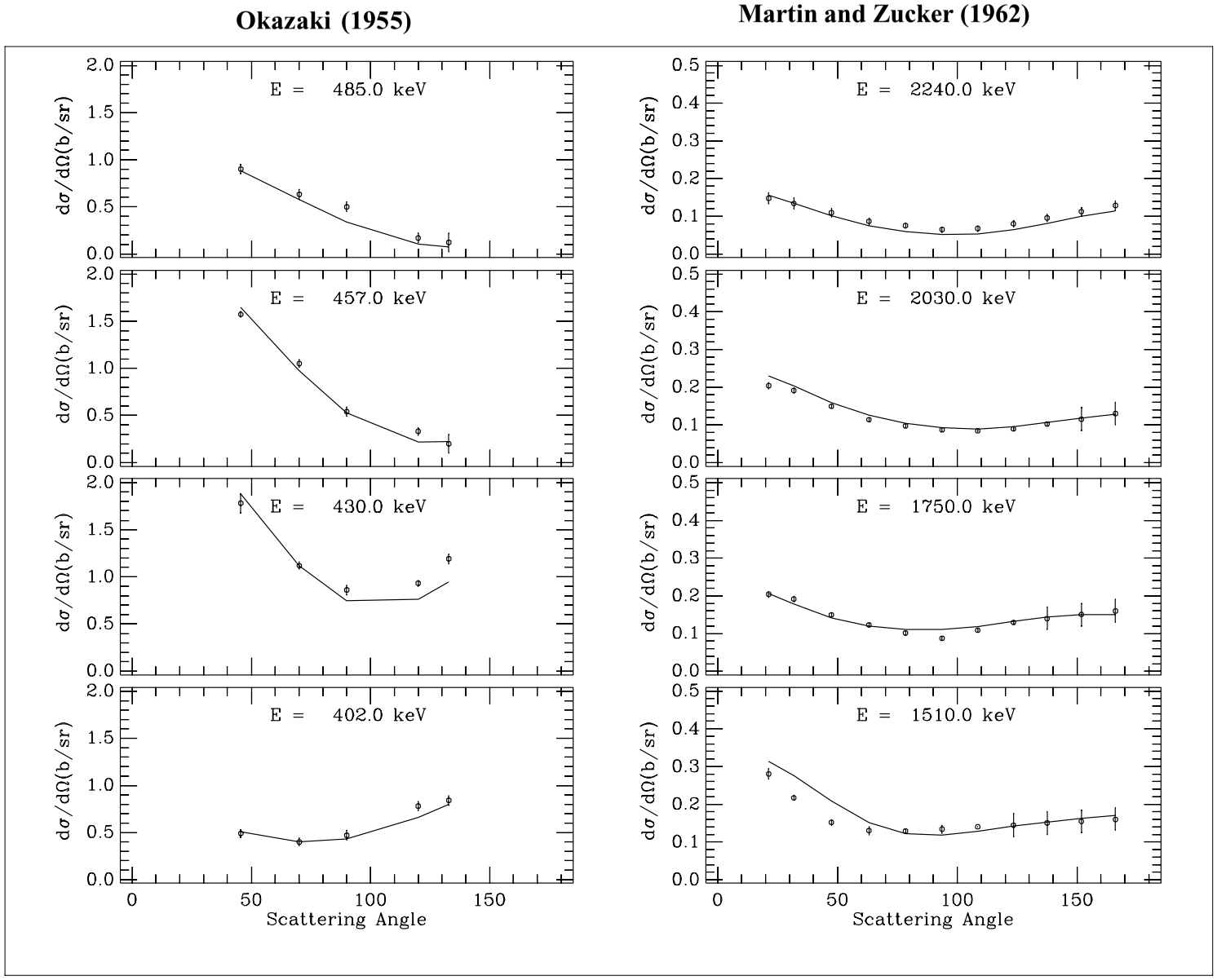

Fig. 9. Comparison of SAMMY predictions to differential elastic data of Okazaki (left frame) and Martin and Zucker (right frame).

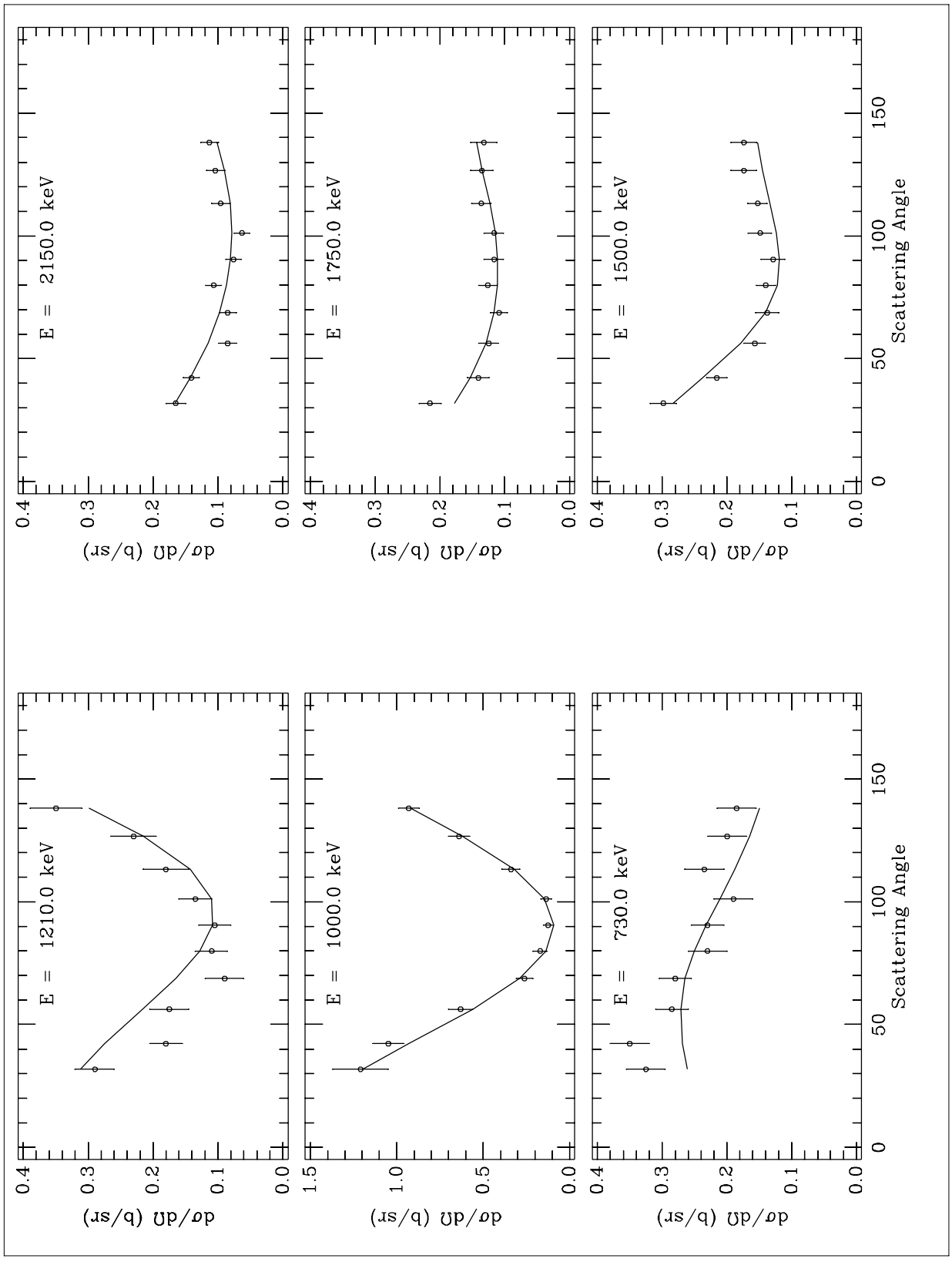

Fig. 10. Comparison of SAMMY predictions to differential elastic data of Fowler and Cohn [FC58].

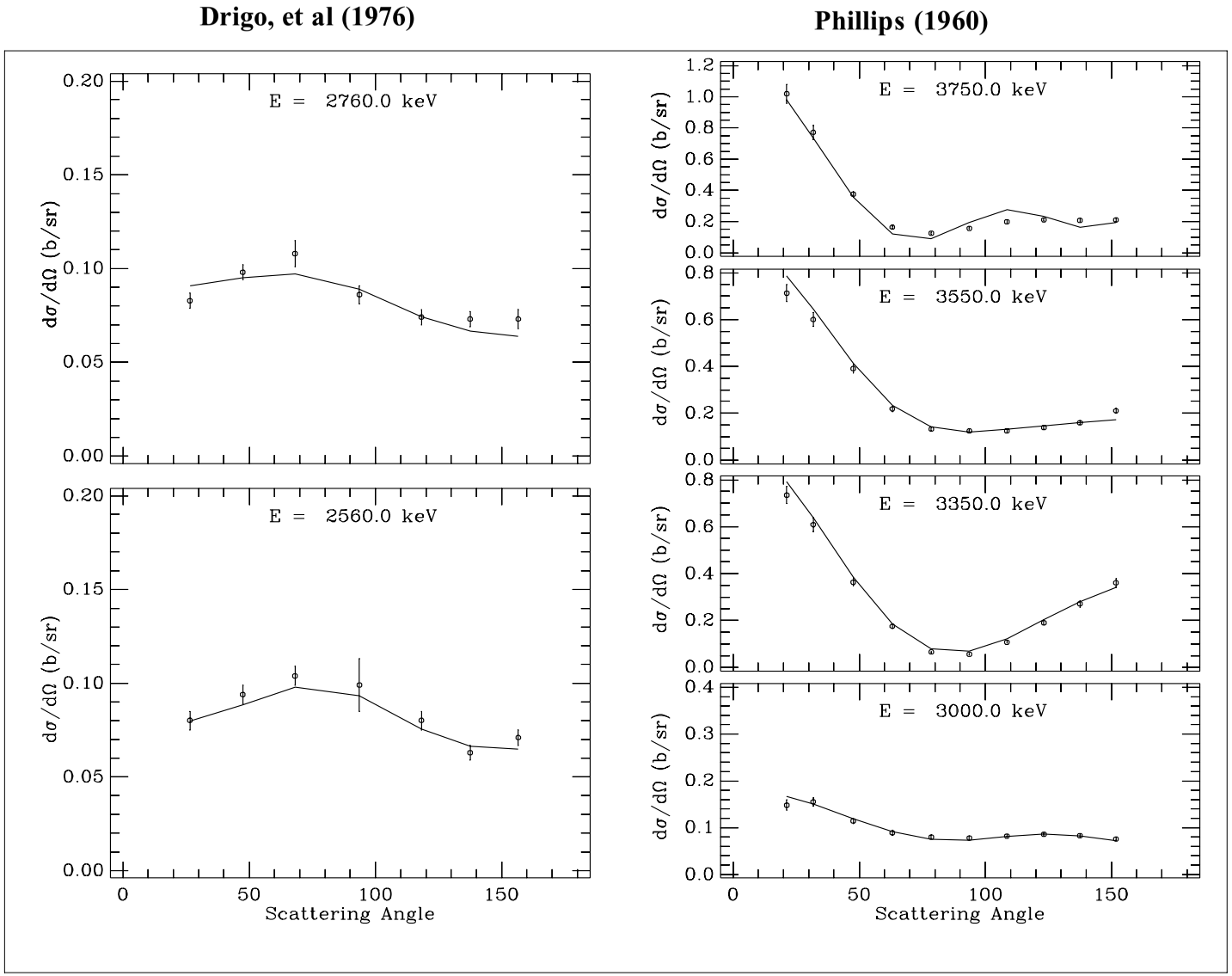

Fig. 11. Comparison of SAMMY predictions to differential elastic data of Drigo, et al (left frame) and Phillips (right frame).

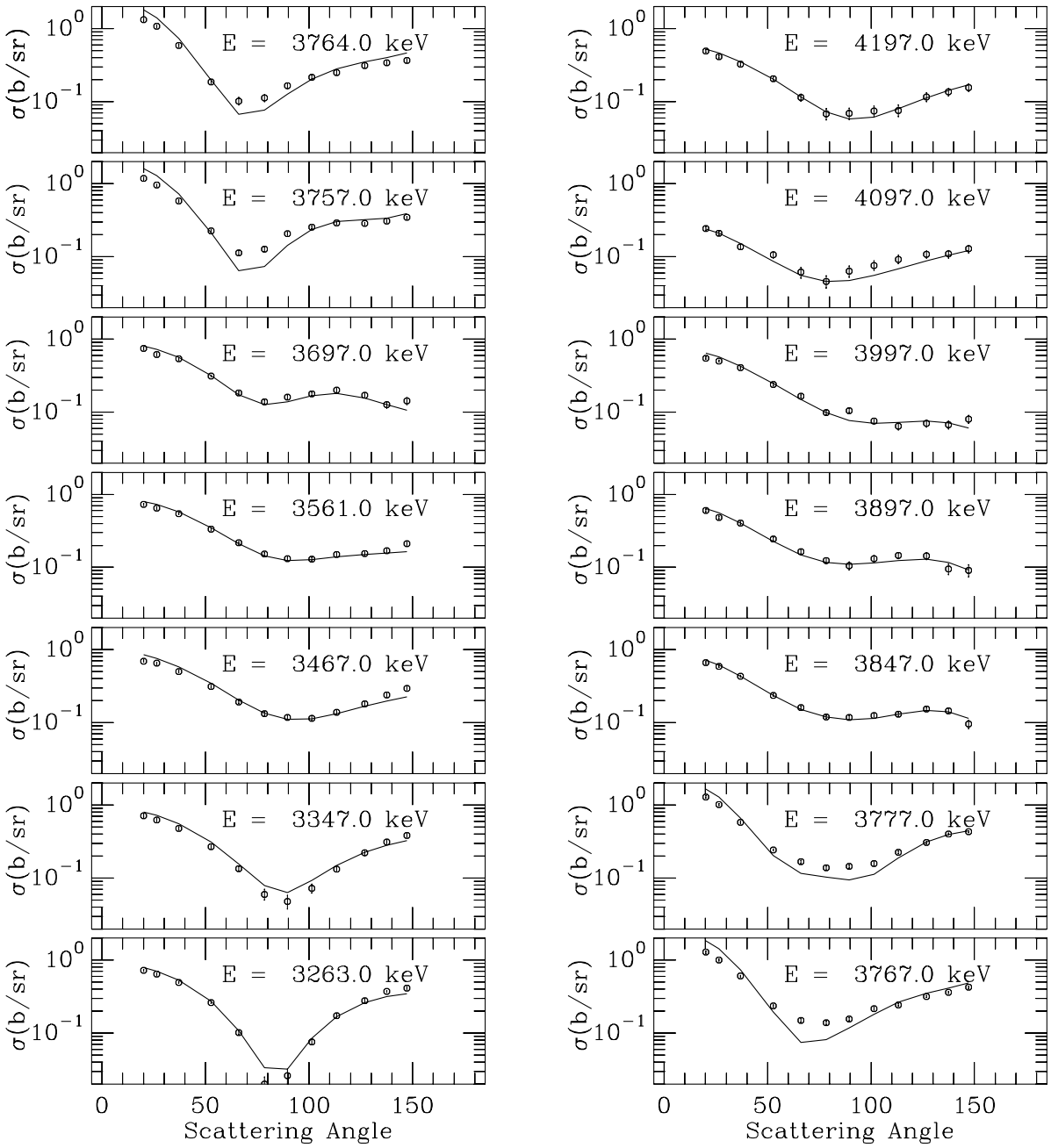

Fig. 12. Comparison of SAMMY predictions to differential elastic data of Johnson and Fowler [JF67].

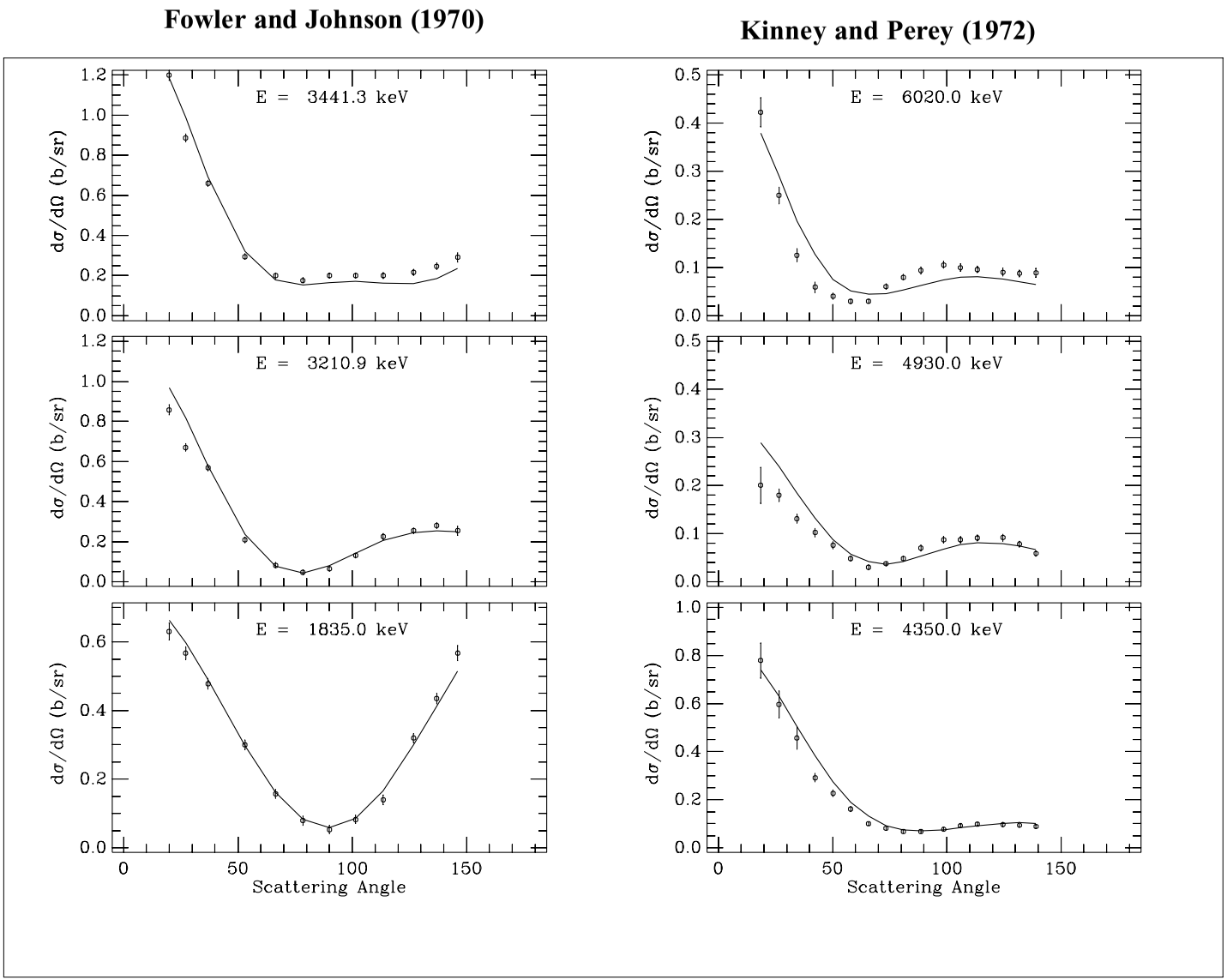

Fig. 13. Comparison of SAMMY predictions to differential elastic data of Fowler and Johnson (left) and Kinney and Perey (right).

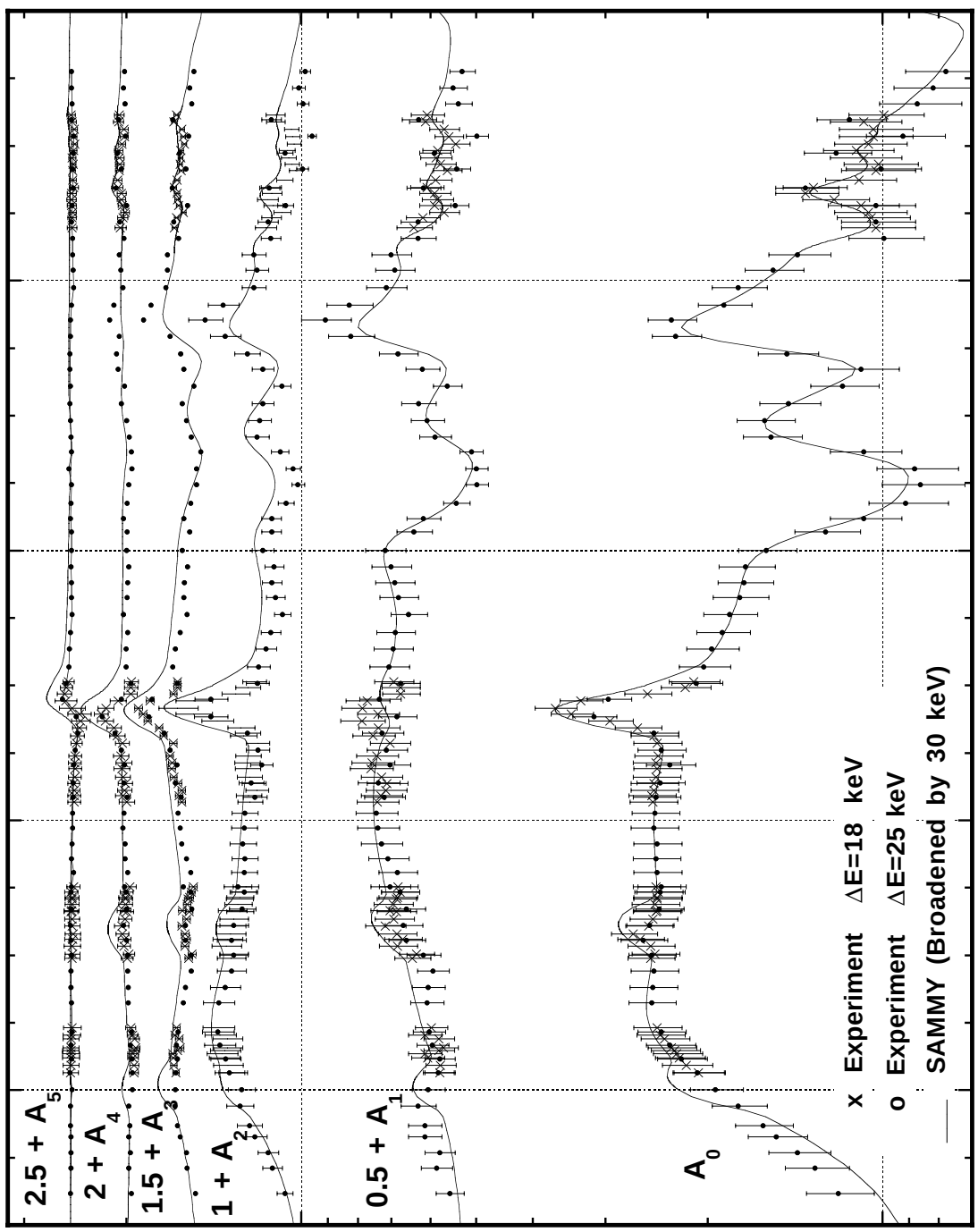

Fig. 14. Comparison of SAMMY predictions to Legendre coefficients of Lister and Sayres [LS66].

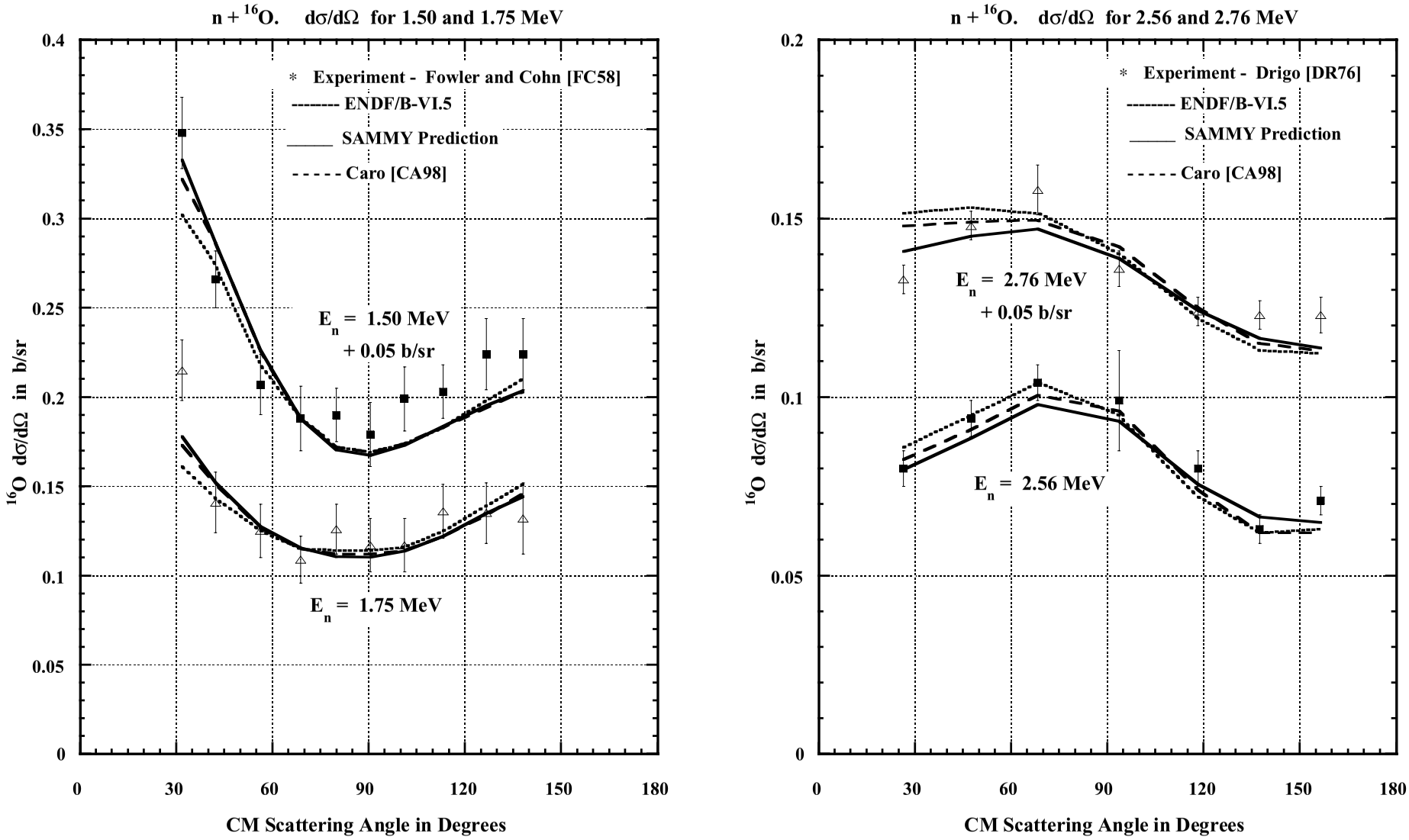

Fig. 15. Experimental, ENDF/B-VI.5, and predicted dσ/dΩ for E_n = 1.50, 1.75, 2.56 and 2.76 MeV

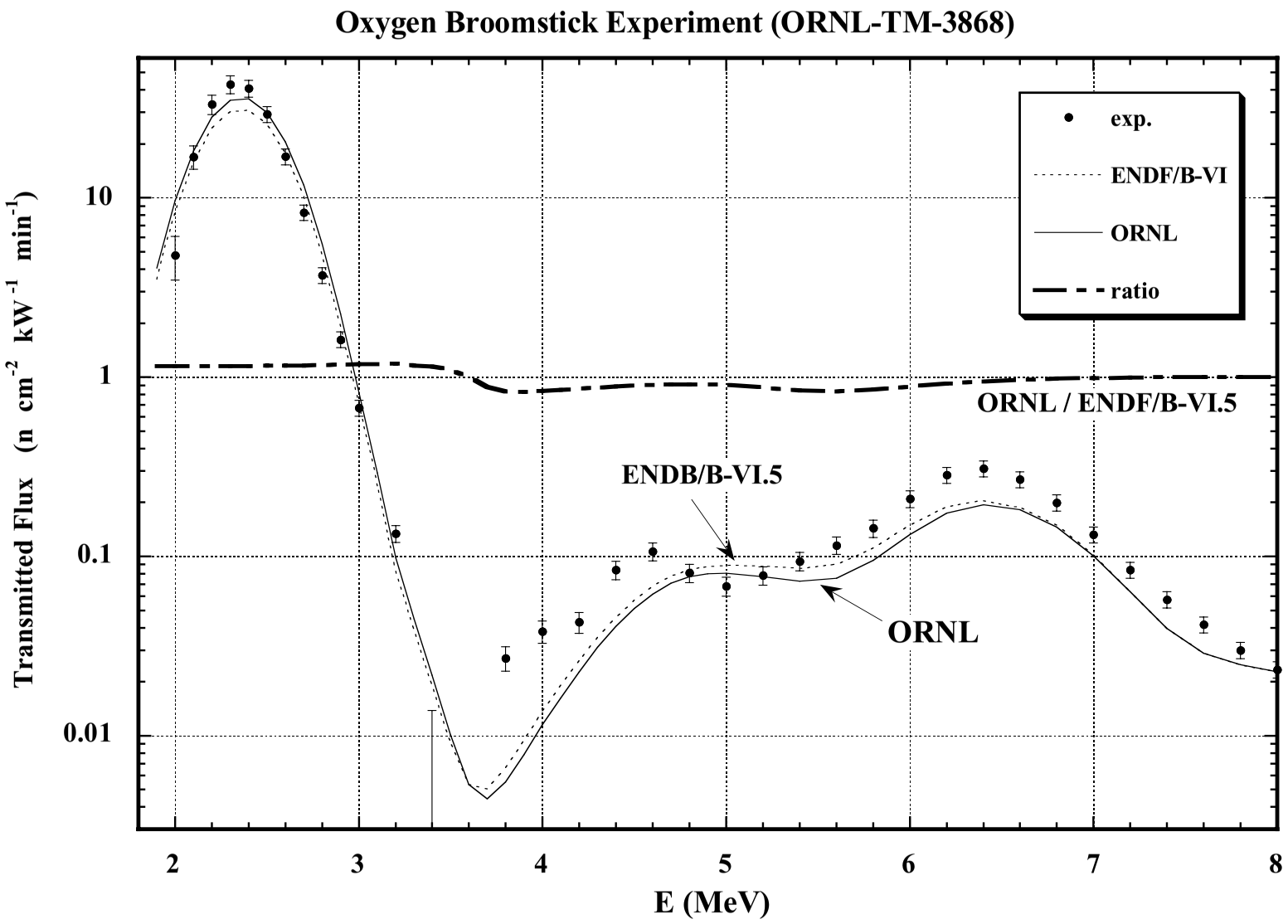

Fig. 16. Comparison of predicted flux to oxygen broomstick experimental flux [MA72].

INTERNAL DISTRIBUTION

1. B. L. Broadhead
2. H. Derrien
3. F. C. Difilippo
4. M. E. Dunn
5. C. Y. Fu
6. N. M. Greene
7. K. Guber
8. F. B. Guimaraes
9. J. A. Harvey
10. C. M. Hopper
11. D. T. Ingersoll
12. P. E. Koehler
13. M. A. Kuliasha
14. D. C. Larson
15. N. M. Larson
16. L. C. Leal
17. S. Y. Oh
18. C. V. Parks
19. S. Raman
20. R. W. Roussin
21-24. R. O. Sayer
25. M. S. Smith
26. R. R. Spencer
27. T. Valentine
28. R. M. Westfall
29. J. E. White
30. R. R. Winters
31. R. Q. Wright
32. RSICC
33. Laboratory Records (OSTI)
34. Laboratory Records
35. Central Research Library

EXTERNAL DISTRIBUTION

36. S. M. Austin, NSCL/Cyclotron Lab, Michigan State University, East Lansing, MI 48824.
37. C. Bastien, Central Bureau for Nuclear Measurements, Steenweg op Retie, 2240 Geel, Belgium.
38. P. Blaise, DER/SPRC/LEPH, Batiment 230, Centre díEtudes de CADARACHE, 13108 Saint Paul-lez-Durance, France.
39. R. Block, Gaerttner LINAC Laboratory, Department of Environmental and Energy Engineering, Rensselaer Polytechnic Institute, Troy, NY 12180-3590.
40. O. Bouland, DER/SPRC/LEPH, Batiment 230, Centre díEtudes de CADARACHE, 13108 Saint Paul-lez-Durance, France.
41. A. Brusegan, Central Bureau for Nuclear Measurements, Steenweg op Retie, 2240 Geel, Belgium.
42. J. Burke, Gaerttner LINAC Laboratory, Department of Environmental and Energy Engineering, Rensselaer Polytechnic Institute, Troy, NY 12180-3590.
43. D. Cabrilla, U.S. Department of Energy, NE-40, 19901 Germantown Road, Germantown, MD 20874-1290.

44. D. E. Carlson, Reactor and Plant System Branch, Division of System Research, Office of Nuclear Regulatory Research, U.S. Nuclear Regulatory Commission, MS T-10 G6, RM T-10, I7, Washington, DC 20555-0001.

45. R. F. Carlton, Department of Chemistry and Physics, Middle Tennessee State University, Murfreesboro, TN 37132.

46. E. Caro, Lockheed Martin Corporation, P.O. Box 1072, Schenectady, N. Y. 12301-1072.

47. D. L. Castro, Physics Education and Engineering Education Departments, Instruction and Training Faculty, California Community Colleges, 1120 Cotton Street, San Diego, California 92102-3639.

48. M. Chadwick, T-2, MS B243, Los Alamos National Laboratory, P. O. Box 1663, Los Alamos, NM 87545.

49. J. Chang, Nuclear Data Evaluation Lab., Korea Atomic Energy Research Institute, P. O. Box 105, Yusung, Taejon, 305-600 Korea.

50. F. Corvi, Central Bureau for Nuclear Measurements, Steenweg op Retie, 2240 Geel, Belgium.

51. D. E. Cullen, MS L-298, Lawrence Livermore National Laboratory, P. O. Box 808, Livermore, CA 94550.

52. Y. Danon, Gaerttner LINAC Laboratory, Department of Environmental and Energy Engineering, Rensselaer Polytechnic Institute, Troy, NY 12180-3590.

53. R. L. Dintaman, U.S. Department of Energy, DP-13, Washington, DC 20585.

54. C. Dunford, Bldg 197D, National Nuclear Data Center, Brookhaven National Laboratory, Upton, NY 11973.

55. J. R. Felty, U.S. Department of Energy, DP-311, Washington DC 20585.

56. P. Finck, Argonne National Laboratory, Reactor Analysis Division, Bldg 208, Argonne, IL 60439.

57. E. Fort, DER/SPRC/LEPH, Batiment 230, Centre díEtudes de CADARACHE, 13108 Saint Paul-lez-Durance, France.

58. N. Francis, Gaerttner LINAC Laboratory, Department of Environmental and Energy Engineering, Rensselaer Polytechnic Institute, Troy, NY 12180-3590.

59. C. M. Frankle, NIS-6, MS J562, Los Alamos National Laboratory, Los Alamos, NM 87545.

60. S. C. Frankle, X-CI, MS F663, Los Alamos National Laboratory, Los Alamos, NM 87545.

61. F. Froehner, Kernforschungszentrum Karlsruhe, Institut fur Neutronenphysik und Reacktortechnik, Postfach 336 40, D-76021 Karlsruhe, Germany.

62. W. Furman, Frank Laboratory of Neutron Physics, JINR, Dubna, Russia.

63. S. Ganesan, Theoretical Physics Division, Central Complex, 5th Floor, Bhabha Atomic Research Centre, Trombay, Mumbai 400 085 INDIA.

64. C. Gould, Physics Dept., North Carolina State University, Box 8202, Raleigh, NC 27695-8202.

65. F. Gunsing, Centre DíEtudes De Saclay, F-Saclay - 91191 GIF-SUR-YVETTE Cedex, France.

66. G. M. Hale, MS B243 T-16 : NUCLEAR PHYSICS , Los Alamos National Laboratory, P. O. Box 1663, Los Alamos, NM 87545.

67. A. Hasagawa, Nuclear Data Center, Japan Atomic Energy Research Institute, Tokai-mura, Naka-gun, Ibaraki-ken 319-11, Japan.

68. R. N. Hwang, Argonne National Laboratory, Reactor Analysis Division, Bldg 208, Argonne, IL 60439.

69. R. P. Jacqmin, DER/SPRC/LEPH, Batiment 230, Centre díEtudes de CADARACHE, 13108 Saint Paul-lez-Durance, France.

70. M. Jaeger, Institut f. Strahlenphysik Allmandring 3 D-70569 Stuttgart, Germany.

71. N. Janeva, Bulgarian Academy of Sciences, 72, Boul, Tzarigradsko shosse, Sofia 1784, Bulgaria.

72. H. C. Johnson, EM-21, Forrestal, U.S. Department of Energy, 1000 Independence Avenue, S.W., Washington, DC 20585.

73. L. Lois, 08 E23, U.S. Nuclear Regulatory Commission, 11555 Rockville Pike, Rockville, MD 20852-2746.

74. G. Leinweber, Gaerttner LINAC Laboratory, Department of Environmental and Energy Engineering, Rensselaer Polytechnic Institute, Troy, NY 12180-3590.

75. R. Little, X-CI, MS F663, Los Alamos National Laboratory, Los Alamos, NM 87545.

76. M. Lubert, Gaerttner LINAC Laboratory, Department of Environmental and Energy Engineering, Rensselaer Polytechnic Institute, Troy, NY 12180-3590.

77. C. Lubitz, Knolls Atomic Power Laboratory, P. O. Box 1072, Schenectady, NY 12301.

78. R. E. MacFarlane, T-2, MS B243, Los Alamos National Laboratory, P. O. Box 1663, Los Alamos, NM 87545-1663.

79. C. Mounier, CEN Saclay, DMT/SERMA/LENR, 91191 Gif Sur Yvette Cedex, France.

80. M. C. Moxon, 3 Hyde Copse, Marcham, Abingdon, Oxfordshire, England.

81. S. F. Mughabghab, Brookhaven National Laboratory, Advanced Technology, Building 197d, Upton, NY 11973-5000.

82. D. Muir, IAEA Nuclear Data Section, Wagramerstr. 5, P. O. Box 100, A-1400 Wien, Austria.

83. J. C. Nimal, DRN/DMT/SERMA, CEA Saclay, bat 470, F-91191 Gif sur Yvette Cedex, France.

84. C. Nordborg, OECD/NEA, Le Seine St-Germain 12, Boulevard Iles, 92130 Issy-les-Moulineaux, France.

85. A. Nouri, OECD/NEA Data Bank, Le Seine Saint Germain, 12, Bd des Iles, 92130 Issy-Les-Moulineaux (France).

86. A. Popov, Frank Laboratory of Neutron Physics, Joint Institute for Nuclear Research, RU-141980 Dubna, Moscow Region, Russia.

87. C. Raepsaet, CEN Saclay, DMT/SERMA/LEPP, 91191 Gif Sur Yvette Cedex, France.

88. M. Salvatores, DRN/P, Batiment 707, C. E. CADARACHE, 13108 Saint Paul-lez-Durance, France.

89. E. Sartori, OECD/NEA, Le Seine St-Germain 12, Boulevard Iles, 92130 Issy-les-Moulineaux, France.

90. O. A. Shcherbakov, Petersburg Nuclear Physics Institute, 188 350 Gatchina, Leningrad District, Russia.

91. R. Shelley, Central Bureau for Nuclear Measurements, Steenweg op Retie, 2240 Geel, Belgium

92. K. Shibata, Nuclear Data Center, Japan Atomic Energy Research Institute, Tokai-mura, Naka-gun, Ibaraki-ken 319-11, Japan.

93. R. Slovacek, Gaerttner LINAC Laboratory, Department of Environmental and Energy Engineering, Rensselaer Polytechnic Institute, Troy, NY 12180-3590.

94. A. B. Smith, TD 362 D216, Argonne National Laboratory, 9700 S. Cass Avenue, Argonne, IL 60439.

95. D. L. Smith, TD 360 L106, Argonne National Laboratory, 9700 S. Cass Avenue, Argonne, IL 60439.

96. H. Takano, Nuclear Data Center, Japan Atomic Energy Research Institute, Tokai-mura, Ibaraki-ken 319-11, Japan.

97. C. Wagemans, Central Bureau for Nuclear Measurements, Steenweg op Retie, 2240 Geel, Belgium.

98. J. J. Wagschal, Racah Institute of Physics, The Hebrew University of Jerusalem, 91904, Jerusalem, ISRAEL.

99. H. Weigmann, Central Bureau for Nuclear Measurements, Steenweg op Retie, 2240 Geel, Belgium.

100. C. J. Werner, Los Alamos National Laboratory, Los Alamos, NM 87545.

101. R. M. White, Lawrence Livermore National Laboratory, P. O. Box 808, Livermore, CA 94550.

102. M. Williams, Nuclear Science Center, Louisiana State University, Baton Rouge, LA 70803.

103. K. Yoo, Nuclear Data Evaluation Lab., Korea Atomic Energy Research Institute, P. O. Box 105, Yusung, Taejon, 305-600 Korea.

104. P. G. Young, MS B243 T-16 : NUCLEAR PHYSICS, Los Alamos National Laboratory, P. O. Box 1663, Los Alamos, NM 87545.